FACTORS CONTROLLING GUIDED CIRCULAR SAW CUTTING BEHAVIOR

by

SHUFAN WANG

B.Sc. Eng., Nanjing Forestry University, 1986

M.Sc. Eng., Nanjing Forestry University, 1989

A THESIS SUBMITTED IN PARTIAL FULFILLMENT OF

THE REQUIREMENTS FOR THE DEGREE OF

MASTER OF APPLIED SCIENCE

in

THE FACULTY OF GRADUATE STUDIES

Department of Mechanical Engineering

We accept this thesis as conforming

to the required standard

THE UNIVERSITY OF BRITISH COLUMBIA

April 1999

In presenting this thesis in partial fulfilment of the requirements for an advanced degree at the University of British Columbia, I agree that the Library shall make it freely available for reference and study. I further agree that permission for extensive copying of this thesis for scholarly purposes may be granted by the head of my department or by his or her representatives. It is understood that copying or publication of this thesis for financial gain shall not be allowed without my written permission.

Department of __Mechanical Engineering__

The University of British Columbia
Vancouver, Canada

Date __April 28, 1999__

DE-6 (2/88)

Abstract

This study consists of an experimental and theoretical investigation of the factors controlling guided circular saw cutting behavior. The work includes preliminary experimental studies, investigation of saw-workpiece interaction mechanisms, saw-workpiece interaction experimental studies and development of a theoretical model.

In the preliminary experimental studies, the fundamental questions are: how do guided saws work, and what are the most significant saw design factors? Extensive experiments were conducted to investigate these questions. A fixed-collar saw closely follows the theoretical expectations. A guided saw only weakly follows theoretical expectations. The interaction between the saw and workpiece was identified as an important factor controlling how guided saws work. It is identified as being a significant saw design factor by experimental observations combined with industrial and previous experiences.

Interactions between the saw and workpiece are identified as key factors controlling guided saw cutting behavior. Two aspects of saw-workpiece interaction are: 1) the interaction between the saw body and the workpiece, and 2) the interaction between the saw teeth and the workpiece. The first interaction type influences the cutting stability of a guided saw compared with a fixed-collar saw. The second interaction type influences the stability of a climb-cutting saw compared with a counter-cutting saw. Extensive cutting tests were performed to explore the effects of the two interaction types. In general, the experimental results supported the theoretical expectations. A guided saw was found to cut more accurately than a fixed-collar saw. A climb-cutting saw was found to cut more accurately than a counter-cutting saw.

A simplified theoretical model of a saw cutting a piece of wood was developed to complement the experimental results and further support the interaction mechanisms. For this model, the practical cutting factors were gradually added to make it more realistic. A computer program was used to implement this model. Typically, this model supports the interaction mechanisms and the experimental results.

TABLE OF CONTENTS

List of Figures

Figures

List of Tables

Tables

Nomenclature

Ω	=	saw rotation speed
ω_s	=	vibration frequency relative to rotating circular saw
ω_b	=	backward traveling wave speed
ω_f	=	forward traveling wave speed
n	=	number of nodal diameters
ΔT	=	temperature difference (amount of tensioning)
$u_1, u_2, ...$	=	vertical linear displacements of nodes
$\theta_1, \theta_2, ...$	=	angular displacements of nodes
$F_1, F_2, ...$	=	vertical forces at nodes
$M_1, M_2, ..$	=	moments at nodes
L	=	length of beam
$L_1, L_2, ...$	=	lengths of beam elements
E	=	material elastic modulus of beam
$E_1, E_2, ...$	=	material elastic modulus of beam elements
I	=	area moment of inertia of beam
$I_1, I_2, ...$	=	area moments of inertia of beam elements
K	=	stiffness matrix
k_f	=	foundation stiffness per unit length
$k_1, k_2, ...$	=	stiffnesses of modeled linear springs at nodes
β	=	numerical coefficient

$v_1, v_2, \ldots$	=	added foundation displacements
H	=	axial force of beam
P	=	axial compressive force
k	=	ratio for beam
P_{CR}	=	Euler buckling load
m	=	mass per unit length
V	=	beam velocity
$\dfrac{D}{Dt}$	=	operator with coordinate system fixed to moving beam
$\dfrac{\partial}{\partial t}$	=	operator for coordinate system fixed in space
x	=	coordinate along length of beam
y	=	coordinate perpendicular to beam
t	=	time
A, B, C, D	=	moving beam equation integration constants
λ	=	equation constant
Δ	=	denominator of terms in stiffness matrix
V_{1stCR}	=	first critical speed of beam element

Acknowledgment

1.0 Introduction

1.1 Background

Profit margin enhancement in saw mills and conservation of limited natural resources urgently demand us to reduce unnecessary wastes during the lumber production process. The raw material alone accounts for around 70-80 percent of the total production cost. Therefore, a major objective that the wood industry is facing is to achieve maximum recovery of high-value products in lumber production.

In most sawmills, circular saws are very important because they process large volumes of wood. At the same time, they create a great deal of sawdust. Further waste is produced by the need subsequently to straighten and smooth the irregular sawn surface by planing. Figure 1.1 shows the practical waste part of one cut. In typical lumber production, sawdust comprises around 15 percent of the total original solid wood. It is almost worthless, and therefore entirely subtracts from the value of the higher-value products that could have been made from the original wood.
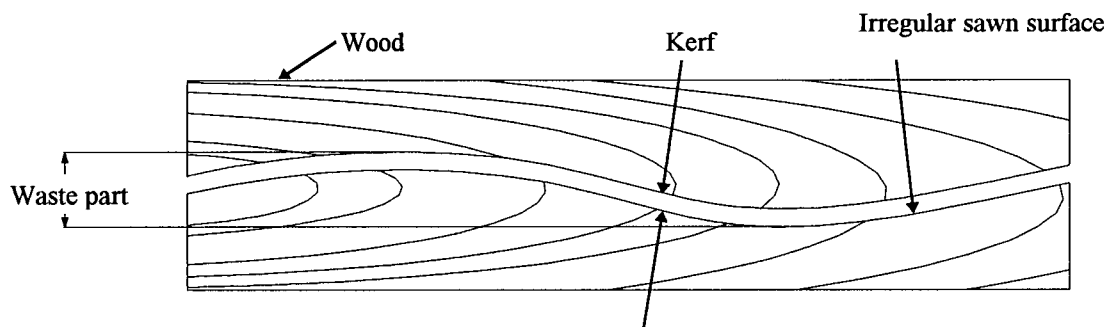
Figure 1.1: Practical Irregular Sawcut

Kerf represents the width of the sawcut as shown in figures 1.1 and 1.2. The amount of sawdust produced corresponds to the volume of the kerf. Cutting accuracy describes the straightness of the sawn wood surface. The width of the irregular sawn surface determines cutting accuracy, as shown in figure 1.1.
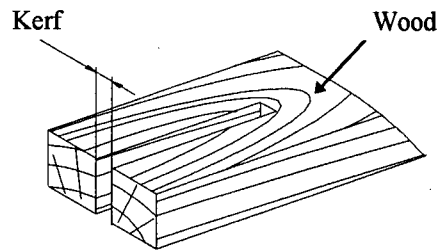
Figure 1.2: Kerf = the Width of Sawcut

According to Maness and Lin's paper in1995 [35], a reduction of 0.01" in the kerf could save around $200,000 per year for a typical sawmill. In 1979, it was estimated that the Weyerhaeuser Company could save around $2 million per year by decreasing 0.01" in kerf in all their sawmills [1]. For this reason, sawmills consider reducing kerf and improving cutting accuracy as major goals in wood production.

In addition to the targets of high recovery and cutting accuracy which most of sawmills are pursuing, productivity, commonly represented by wood feed speed, is also an important industrial practical need.

Usually, to a great extent, recovery, accuracy and productivity conflict with each other [2]. Improving one can impair one or both of the other two factors. For example, increasing productivity typically decreases accuracy and recovery. Use of a modern type of saw, the guided circular saw, provides an effective way of improving all three factors simultaneously.

There are two main types of circular saws, fixed-collar saws and guided spline-arbor saws. These are shown in figure 1.3(a) and (b). The former has a fixed collar at the center of sawblade and is the traditional saw type. The latter has a guide near its cutting area to restrict the axial lateral motion of the sawblade and is the more modern saw type.

Figure 1.3(c) shows a sketch of a climb-cutting saw vs. a counter-cutting saw. For a climb-cutting saw, the tooth cutting direction is opposite to the feed direction of wood at

the cutting area. This is the traditional arrangement. For a counter-cutting saw, the tooth cutting direction coincides with the feed direction of wood at the cutting area.

Cutting area   Spline-arbor

Fixed collar

Guide

Sawblade

(a) Fixed Collar Saw   (b) Guided Spline-arbor Saw

Counter-cut

Wood

Sawblade

Spline-arbor

Climb-cut

Guides

Wood

(c) Counter-Cutting Guided Saw and Climb-Cutting Gudied Saw
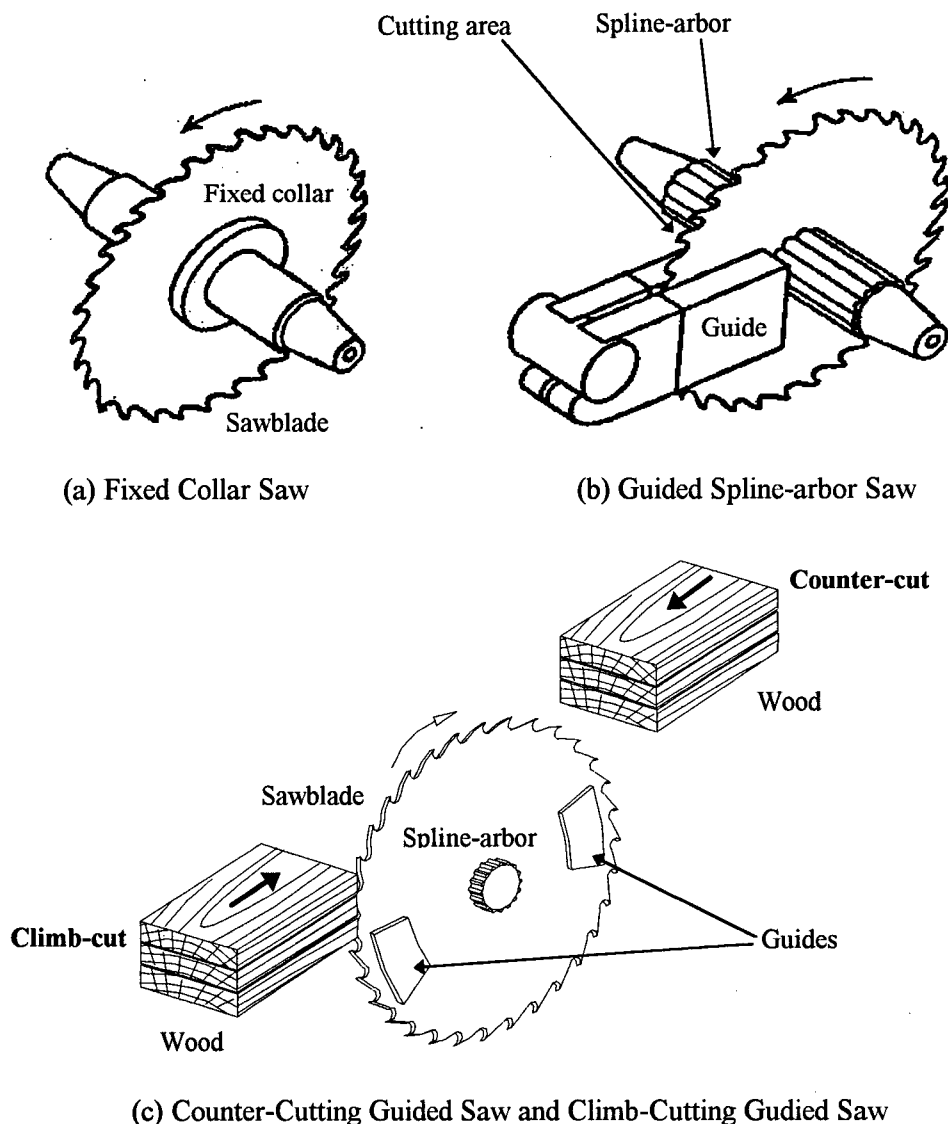
Figure 1.3: Saw Types

Over the last thirty years, guided spline-arbor saws have been used extensively in North American sawmills. In almost all new gangsaw installations, traditional fixed-collar saws have almost entirely been replaced by guided saws [3]. The main reason is that guided saws can produce superior cutting accuracy and much smaller kerf at practical feed and

cutting speeds. Lumber production industries can therefore get the best economic trade-off between lumber recovery and production rates [4].

In practical lumber production, some care must be given when reducing saw plate thickness as a means of reducing kerf. A thick sawblade has a good capacity to tolerate imperfections in the sawing process such as machine misalignments and non-ideal saw tensioning, leveling and sharpening. A thick sawblade can cut stably despite such imperfections. The presence of the imperfections is therefore not apparent. However, a thin saw has much less capacity to tolerate sawing process imperfections. Thus, a change to a thinner saw can reveal sawing process imperfections that were not previously apparent. A change to a thinner saw requires that increased attention be given to machine alignment and saw maintenance. Otherwise, the kerf gain achieved by reduced plate thickness will be lost by reduced cutting accuracy.

Even though guided saws are most prevalent in North American sawmills, the reason for the superior cutting of guided saws has not clearly been explained by a convincing theory. Practical sawing and saw design can still be further advanced by more fully understanding the key factors that affect guided saw cutting behavior. This is the motivation for this thesis. It is hoped that the results of this thesis may also give benefit to the developing countries where fixed-collar saws are prevalent or use of guided saws is in its initial stage.

Guided spline-arbor saws possess many geometric similarities to fixed-collar saws. The reason why guided spline-arbor saws give superior cutting when compared with fixed-collar saws has attracted a large amount of research effort aimed at machine understanding and improvement [3]. From the point of view of design, the benefits from the thinner kerf and the superior cutting accuracy of guided spline-arbor saws more than compensate for the increased machine complexity caused by the additional guides. In brief, the fundamental questions of interest are: how do guided saws work, and what are the most significant saw design factors?

The key to the settlement of these questions lies in fully understanding the factors controlling guided circular saw cutting behavior. Firstly, a preliminary understanding of the following three key concepts is helpful to investigate these factors:

1. Critical speed instability
2. Saw tensioning
3. Saw dishing

1.2 A Preliminary Understanding of the Key Concepts

Critical Speed Instability

Critical speed instability describes the concept concerning an unstable and unfavorable behavior of saw which corresponds to a special rotation speed called the "critical speed". At the critical speed, a vibration resonance condition occurs, where the unstable sawblade slowly moves from side to side, and causes the "snaking" sawcuts with "wave" profile shown in figure 1.1 [6]. One can imagine that if practical wood sawcuts were like this, how much solid wood would be wasted in lumber production!

The traditional critical speed theory of fixed-collar saws is based on this unstable threshold. When the operating speeds of fixed-collar saws are above or near the critical speed, sawblades become very unstable. A further description will be presented in Chapter 2.

The critical speed of a sawblade is proportional to its plate thickness [4, 5, 6, 8]. Therefore, kerf reduction is limited by the minimum allowable critical speed of the sawblade. This effect can be mitigated by using saw tensioning, which has the effect of increasing the critical speed.

Saw Tensioning

Saw tensioning is a process by which in-plane stresses, "tensioning stresses", are deliberately put into a sawblade by using methods such as hammering, rolling or non-uniform heating [6]. Saw tensioning is an effective method to increase critical speed and

minimize the possibility of snaking sawcuts. However, over-tensioning can cause sawblade dishing as shown in figure 1.4.
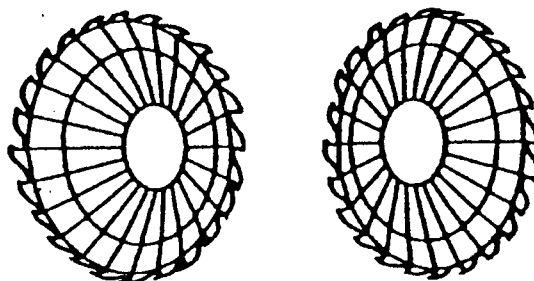
Figure 1.4: Saw Dishing

Saw Dishing

Dishing is the name given to saw plate buckling caused by compressive radial in-plane stresses. The dished sawblade shown in figure 1.4 can produce tapered lumber, as shown in figure 1.5. Dishing also makes leveling a sawblade on the workbench more difficult. Therefore, saw dishing is generally avoided in practice.
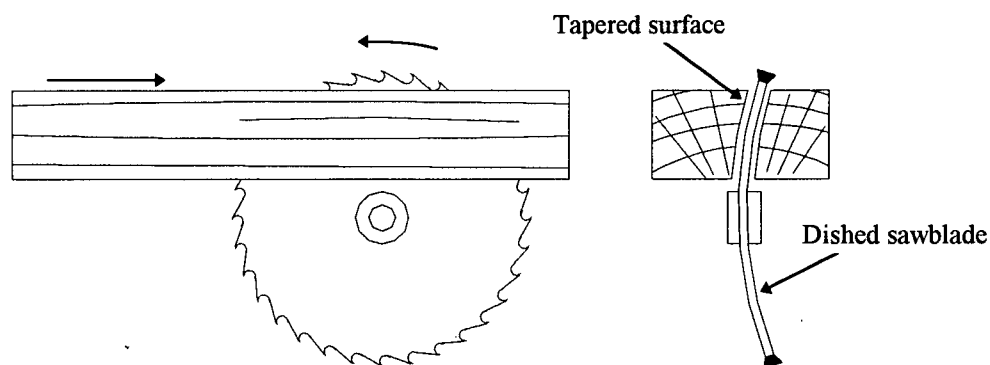
Figure 1.5: Tapered Lumber

1.3 Previous Research

Campbell's [7] research in the 1920's on the subject of turbine disc wheels was one of the first significant contributions to the field of rotating disk vibration. He concluded that a non-uniform axial static pressure around the circumference excited a standing wave at a resonant speed called the critical speed, leading to failure of steam turbine discs. A

diagram called the Campbell Diagram, with the rotation speed as abscissa and the natural frequency as ordinate, was first used to analyze the relationship between the natural frequencies and rotation speed of disc. Now this diagram is used as a tool to analyze the natural frequencies and critical speed of circular saws.

Dugdale [5] developed the theory of circular saw stability based on the previous theory of spinning discs. In 1966, he studied the stiffness of a spinning disc clamped at its center. In his studies, the minimum critical speed of the discs at which their stiffnesses reduced to zero was examined both theoretically and experimentally. He considered the factors of disc thickness, collar and outside diameters and disc tensioning as the main influences on the disc critical speeds.

Mote [8-12] also applied the previous theory in the field of rotating discs to circular saw stability research. In his work [8] in the 1960's, he analyzed the fixed-collar circular saw stability problem by considering the factors of bending stiffness, thermal gradients, angular velocity and tensioning stresses. In 1970 [9], he investigated the stability of circular plates subjected to moving loads by using an eigenvalue analysis and spectral analysis experiments. Finally he remarked that the critical speed instability condition, which results from a variation of the membrane stress state, is predictable from the subcritical spectral analysis. In 1977 [10, 11], Mote and Szymani identified influencing factors such as the saw geometry, clamping ratio, material properties, the membrane stresses, process parameters and aerodynamic vibration. Some design factors, such as tapered saws, saw slots and guides were also investigated. Using the critical speed as a stability measure was the main trend of this future research. They also first introduced the idea of interaction of the workpiece with the saw lateral surfaces. At that time, the interaction was considered as random force causing variations in saw vibration. The critical speed instability was considered the most significant concept and had precedence over other concepts such as buckling etc. In 1981 [12], Mote, Schajer, and Holøyen experimentally found that sawblade temperature control was an effective method of controlling both the sawblade vibration and the product thickness variation in blade designs.

Schajer [13, 14, 15, 16, 3] also devoted much of his work to the field of guided circular saw cutting stability, based on the previous unguided saw theory. In 1984 [13], Schajer found a design factor influencing the accuracy of lateral positioning of a guided circular saw, hunting instability, which was controlled by position of guides, saw rotation direction and area of contact between sawblade and drive shaft. In 1986 [14], he introduced lateral stiffness as a stability measure. A guide close to the cutting zone can make sawblade resist greater lateral cutting forces. Proper tensioning also can maximize saw stiffness. He also remarked that previous traditional critical speed theory and lowest natural frequency theory can not sufficiently explain the behavior of guides, and can underestimate the beneficial effect of guide. In 1989 [15], he gave an insight into guided circular saw critical speed by using experimental work based on traditional critical speed theory. He concluded that guides had very little effect on the critical speed except for complicating sawblade vibration. The purposes of guides were to provide lateral support close to the cutting area, damping and saw cooling. In 1991 [16], Schajer theoretically analyzed the complex vibration behavior of a guided saw. In 1997 [3], Schajer and Kishimoto investigated the idling and cutting behavior of guided circular saw by doing experimental observations. The behavior of an idling guided circular saw closely followed the expectations of classical critical speed theory, but sawblade cutting behavior was significantly different. This observation confirmed industrial experience where operating speeds above the first critical speed were used. Finally they concluded that the interaction between the workpiece and the saw was a key factor affecting saw cutting behavior.

Hutton [17-20] also did extensive research in the field of circular saw cutting stability. In 1987, Hutton etc. [17] developed a theoretical model to investigate the dynamics of guided rotating discs and guided circular saws. They also concluded that the introduction of one or two guides did not significantly influence the critical speeds of sawblades. In 1988 [18], Lehmann and Hutton investigated the vibration behavior of guided rotating saws that were not perfectly flat by using experimental and analytical methods. They found that when sawblade was not perfectly flat, a self-excited resonance could occur at certain speeds by the interaction between the guides and the sawblade. Self-excitation can

be avoided by adjusting the speed, changing the tensioning, minimizing sawblade runout, or by using guide arms that have high natural frequencies. In 1991 [19], Hutton reviewed the knowledge of vibration characteristics of fixed-collar circular saws and guided circular saws, and provided analytical and experimental results. He described that the mechanisms that govern the interaction between wood and sawblade were known incompletely and operation of saws in the supercritical speed range was of an interest. Finally he concluded that design of optimum guide configuration selection was needed. In 1995 [20], Yang and Hutton further developed the model of an idealized rotating circular string and a stationary constraint first introduced by Schajer [22]. By using eigenvalue analysis, finally they obtained several important results concerning different constraints such as mass, damping and friction.

Lister [4] is also an active researcher in the field of circular saw cutting stability. In 1997, he did laboratory tests to investigate the supercritical speed behavior of guided circular saw designs used by industry. The tests of three thicknesses of guided circular saws and two supercritical speed circular saw configurations were conducted in idling tests and in cutting tests respectively. Experiments showed that the guided circular saws used by industry could successfully operate at supercritical speeds. Although these saws were much thinner than conventional saws, they can give acceptable sawing accuracy. Experiments also showed that the sawcut accuracy or sawing stability was influenced by the factors of blade thickness and feed speed.

As mentioned above, many previous guided saw studies have focused on the vibration characteristics of guided saws. These vibration studies commonly use eigenvalue analysis with models that incorporate various features of guided saws. The starting point of these vibration studies is the traditional critical speed theory, which successfully explains the behavior of fixed-collar saws. In fact, a guided saw has either the same or lower critical speed as a fixed-collar saw of the same dimensions [15]. Thus, on the basis of the traditional critical speed theory, a guided saw should need a larger plate thickness for the same cutting accuracy. The previous theoretical and experimental studies have indicated

that the traditional critical speed theory is not adequate to explain the cutting behavior of guided saws [3, 14].

In the process of investigating the behavior of guided saws, the interaction between workpiece and saw was identified as a factor by some previous researchers [10, 19], but this factor has not been given much attention so far. A recent article [3] considered this interaction as a key factor in the cutting of guided saws in the experimental observations, and anticipated more experimental and theoretical work to provide verification. The practical industrial operation of guided saws at supercritical speeds, as indicated in the experimental studies [4], also suggests that the interaction is an important factor controlling guided saw cutting behavior.

There may be two reasons why many circular saw studies do not give emphasis to this factor. Firstly, there is incomplete knowledge of its mechanisms. Secondly, much research uses eigenvalue analysis, but it is difficult to do an eigenvalue analysis with a dynamical model that describes the interaction between the workpiece and the saw realistically.

For these reasons, this study will use a time domain analysis of the factors controlling guided saw cutting behavior. This work will be complemented by extensive experimental studies.

1.4 Objectives and Scope

The objectives of this research work are to understand the factors controlling guided circular saw cutting behavior and to provide insight into the design of improved guided circular saws.

The procedures used in this study to achieve its objectives are:

1. Investigate the theoretical background.

2. Conduct preliminary experimental studies by considering how closely practical guided saw behavior compares with the expectations from the traditional critical speed theory. Use the experimental results to investigate the fundamental questions: how guided saws work, and what the most significant saw design factors are. The following four steps are needed:

   - Conduct initial idling tests using a fixed-collar saw to observe the original saw behavior that matches the traditional critical speed theory.

   - Perform fixed-collar saw cutting tests and observe the cutting behavior. Compare the cutting fixed-collar saw results with the idling saw results to determine how well the fixed-collar saw behavior follows the traditional critical speed theory. Use the fixed-collar saw results as "base case".

   - Do guided saw cutting tests and observe the cutting behavior from the same sawblade used for the fixed-collar saw tests. Compare the guided saw results with the "base case" to determine how closely the guided saw behavior compares with the expectations from the traditional critical speed theory.

   - Combine previous guided saw idling test results [3] with the results of a comparison between the guided saw results and the fixed-collar saw results to investigate the fundamental questions.

3. Investigate the interaction of the workpiece with the saw as a key factor controlling guided saw cutting behavior.

4. Develop simple geometrical interaction mechanisms based on practical experimental observations and results.

5. Design and conduct the second stage experimental studies to examine how the interaction mechanisms work by doing following three steps:

   - Conduct initial idling tests using a guided saw with the same sawblade to get the idling guided saw behavior.

   - Design cutting tests with different guide configurations and cutting directions based on the interaction mechanisms.

   - Perform cutting tests and analyze the results to determine whether interactions between workpiece and saw are major factors controlling guided saw behavior.

6. Develop a theoretical model of a saw cutting a piece of wood to support the interaction mechanisms and complement the experimental results. In this model, the evolution of the interaction of the saw with the workpiece will be shown by a time-based iteration. Finally this model will become a more realistic and general form by adding necessary saw cutting factors.

7. Examine the theoretical model behavior which will be compared with the practical cutting test behavior of the guided saw. Finally reconfirm that the factors controlling guided saw cutting behavior are the interactions between workpiece and saw.

This sequential approach is designed to provide insight into the interaction between the workpiece and saw. Experimental observations give some significant inspirations to us to find this key factor. Extensive experiments cover a testing range as large as possible to investigate the fundamental questions. Simple geometrical interaction mechanisms and further experiments support the hypothesis and give the basis to build a theoretical model. The theoretical model will complement the extensive experiments and further support the belief that the interaction between the workpiece and saw is a key factor controlling guided circular saw cutting behavior.

2.0 Theoretical Background

The three key concepts, critical speed instability, tensioning and saw dishing, were briefly mentioned in the Introduction. In this chapter, the physical meanings of these three key concepts will be clarified further, and their expected interactions will be described using a diagram based on the classical critical speed theory for a fixed-collar circular saw. The theoretical background summarized here is mainly based on the articles [2, 15, 3, 10, 6].

2.1 Thin Circular Saw Vibration

When a fixed-collar saw cuts wood, saw vibration is inevitable because of sawblade runout, natural differences in the wood boards, unsymmetrical saw teeth, machine alignment and so on. A circular saw vibrates at various natural frequencies, each corresponding to a different vibration mode shape. Vibration modes can be described by the number of nodal diameters, as shown in figure 2.1.

0 Nodal diameters   1 Nodal diameter   2 Nodal diameters   3 Nodal diameters
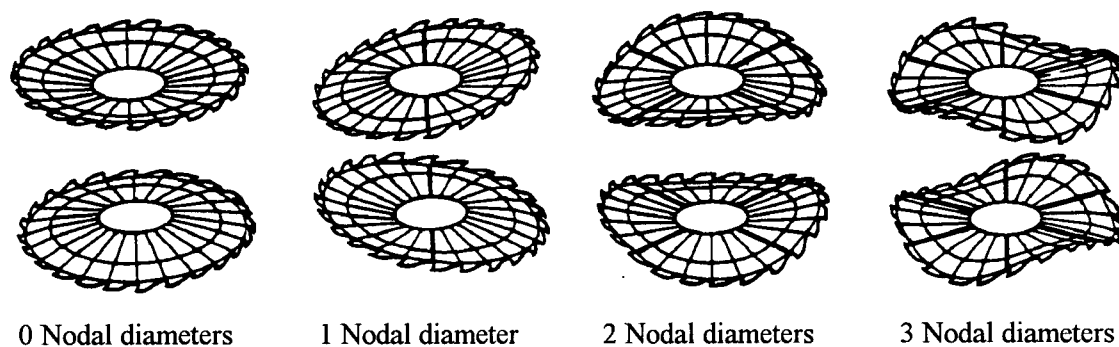
Figure 2.1: Vibration Modes of a Circular Saw. From Schajer [15].

Figure 2.1 shows standing wave vibration of a stationary sawblade. Another way of describing sawblade vibration is as the sum of two similar traveling waves moving at the same speed in opposite directions around the saw. Since these waves move at the same speed, they have the same frequencies. When the saw rotates, the rotation speed of the saw adds to one traveling wave speed and subtracts from the other. The two waves then

have different speeds when observed by a stationary observer. These different wave speeds cause corresponding changes in the observed frequencies. Figure 2.2 shows a diagram of traveling wave frequencies vs. rotation speed of a circular saw. A rotation speed Ω will increase the forward traveling wave speed by $n\Omega$ and decrease the backward traveling wave speed by $n\Omega$. The vibration frequencies are given by the following equations.

Backward traveling wave speed: $\omega_b = \omega_s - n\Omega$

Forward traveling wave speed: $\omega_f = \omega_s + n\Omega$

$$(2.1)$$

where ω_s is the vibration frequency relative to rotating circular saw, Ω is the circular saw rotation speed, and n is the number of nodal diameters.
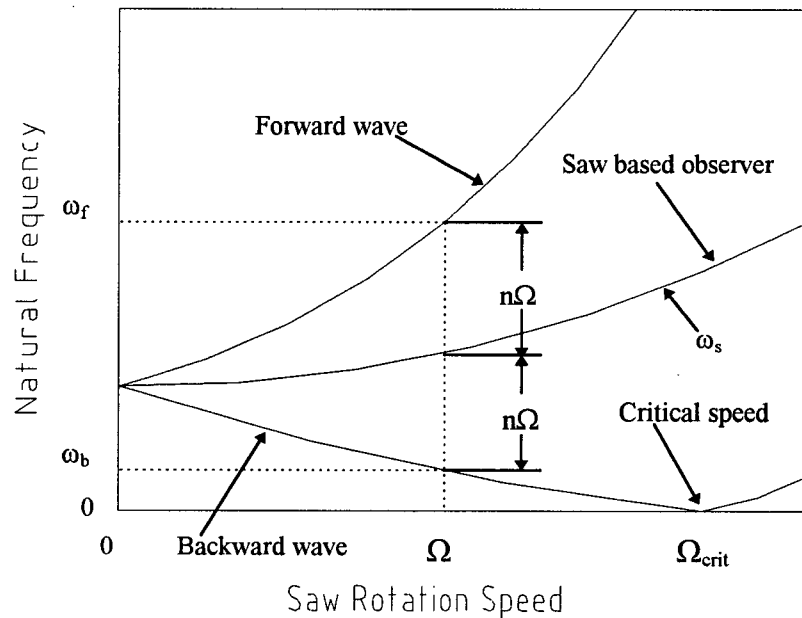
Figure 2.2: Traveling Wave Frequencies of a Circular Saw

2.2 Critical Speed Instability

The saw rotation speed subtracts from the backward traveling wave speed. At the "critical speed", when the saw rotation speed equals the traveling wave speed, the backward traveling wave has a zero net speed. The corresponding frequency is also zero. Theoretically, the mode shape at the exact critical speed would appear to be a fixed

profile. In reality, a sawblade does not rotate at the exact critical speed. Therefore, the practical wave of the mode shape seems to move slowly around the sawblade. A snaking sawcut results from this unstable behavior of the sawblade moving from side to side in the sawcut.

All vibration modes shown in figure 2.1 except the zero nodal diameter vibration mode possess their own different traveling wave frequency diagrams similar to the one shown in figure 2.2 and their own critical speeds corresponding to the points of zero backward traveling wave frequency. Since the operating speeds of unguided saws are near and below the lowest critical speed, the lowest critical speed is the most significant one. The critical speed usually occurs in the two, three or four nodal diameter vibration modes shown. In general, for unguided circular saws, the concept of the critical speed focuses on the lowest critical speed.

The critical speed of a thin saw decreases with reducing the thickness of the sawblade. Therefore, for thinner sawblade thickness, the sawn surface quality is impaired by frequent snaking sawcuts because the saw operating speed more easily approaches the lowest critical speed

2.3 Tensioning

As mentioned in the introduction, saw tensioning is a useful method of increasing critical speed and avoiding snaking sawcuts. Saw tensioning consists of in-plane stresses that are purposely produced in the sawblade by the methods of hammering, rolling or non-uniform heating. Hammering involves using a hammer to plastically deform the sawblade surface slightly to produce locked-in (residual) stresses. Rolling involves squeezing the saw between two rollers and creating a circular track around the saw surface. It is generally a superior process because it produces more uniform results. Non-uniform heating involves heating the center of the sawblade to produce a thermal stresses due to the temperature difference between central area and the outer rim. The advantage of this method is that the size of the induced thermal stresses (the "thermal" tensioning) can be easily adjusted

by controlling the amount of the heating. In the practical experiments described in this thesis, non-uniform heating will be used to build different temporary tensioning to explore the behavior of the saw. This temporary tensioning disappears when the heating is removed.

Proper tensioning can produce tensile stresses that can stiffen sawblades and accordingly increase the critical speeds of the saws. It therefore makes the use of thinner sawblades possible. However, the amount of tensioning is restricted by sawblade dishing shown in figure 1.4.

2.4 Saw Dishing

As mentioned in the Introduction, saw dishing corresponds to sawblade buckling. It is produced by compressive radial stresses.

From the point of view of vibration modes, over-tensioning makes the zero nodal diameter mode vibration frequency become equal to zero. Consequently the dished saw takes the zero diameter mode shape shown in figures 1.4 and figure 2.1. This dishing causes the saw to produce the undesirable tapered lumber shown in figure 1.5.

When saw dishing occurs, the surface profile of the sawblade is no longer flat and looks like a shallow "bowl". Excessive tensioning will make the "bowl" deeper. Consequently, sawblade maintenance such as leveling is more difficult due to the dished saw being unable to lie flat on the workbench. In practice, saw dishing can serve as the method to measure the amount of tensioning by placing a straight-edge across the saw diameter [23].

In the experiments described in this thesis, dishing is sometimes created by the thermal tensioning. When the sawblade rotates, the tensile rotational stresses counteract the compressive radial tensioning stresses and draw the dished sawblade back to a flat surface profile. The speed at which a dished sawblade becomes flat is called the dishing speed.

2.5 Relationship of The Critical Speed Instability, Tensioning and Dishing

Figure 2.3 depicts a combination diagram illustrating the relationship between the three key concepts, critical speed instability, tensioning and saw dishing. This diagram, which plots the saw rotation speed vs. the amount of tensioning, shows two curves and three areas. They are the critical speed curve, the dishing speed curve, the snaking saw area, the dished saw area and the stable saw area. In this diagram, the abscissa ranges from zero saw tensioning on the left to high saw tensioning on the right.
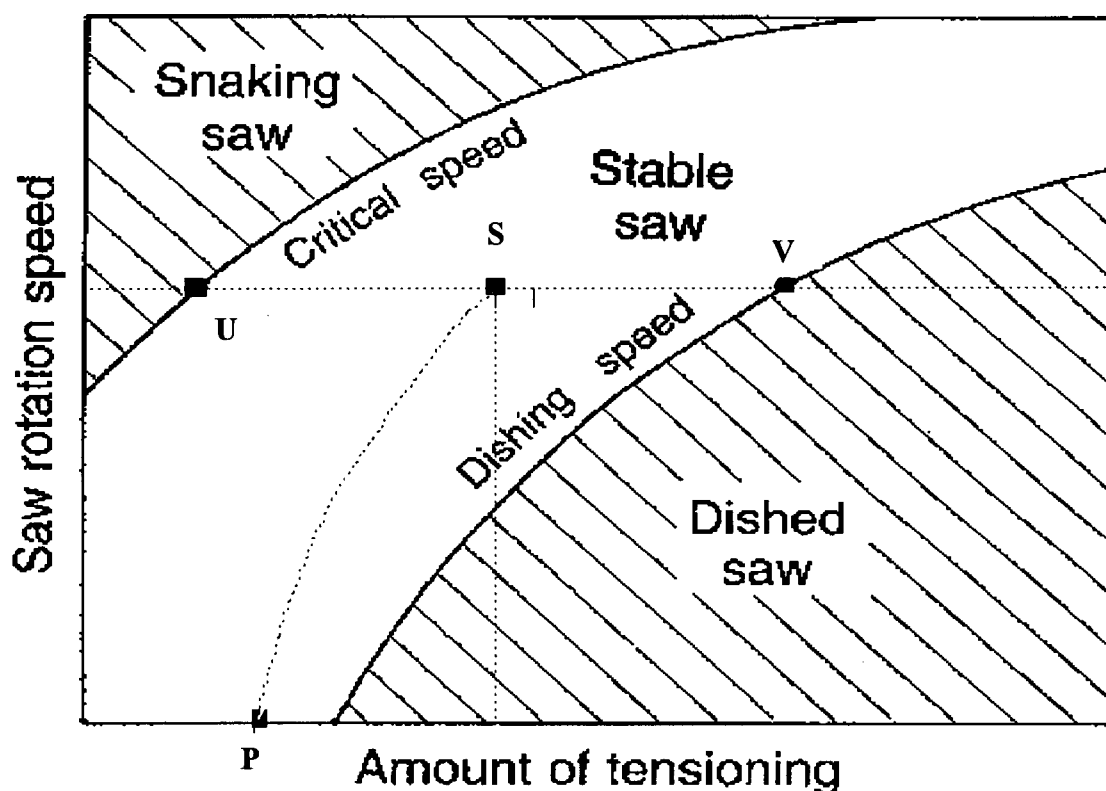
Figure 2.3: Relationship between the Critical and Dishing Speeds of a Fixed-Collar
Circular Saw and the Amount of Tensioning

The upper curve, called the critical speed line, clearly illustrates how the critical speed of a fixed-collar saw increases with saw tensioning. When the operating speed of a fixed-collar saw is close to this curve, unstable vibrational resonance will occur, resulting in snaking sawcuts. Since saw rotation speeds above the critical speed curve include many other critical speeds with corresponding nodal diameter vibration modes, all operating speeds in

this upper area lead to snaking sawcuts with a fixed-collar saw. Therefore, the upper shaded area above the critical speed curve, called the "Snaking saw" area, is unfavorable for practical lumber production. The greatly increasing critical speed with increasing saw tensioning provides a better condition of promoting operating speeds to achieve higher productivity by using thin circular saw. Therefore, substantial tensioning is desirable. However, dishing limits the amount of tensioning that can be used in practice.

The lower curve, called the dishing speed line, provides a lower bound for a saw keeping accurate sawcut at its operating speed. The tensile stresses created by the saw rotation centrifugal force will counteract dishing. When the operating speeds of a fixed-collar saw exceed the dishing speed curve, the tensile rotation stresses counteract the dishing and pull the curved plate back to the flat plate. Therefore, the sawcuts are accurate. The dishing curve also shows the increase of dishing speed with the increase of tensioning and the greater tensioning required by higher operating speeds.

The middle unshaded area in figure 2.3, called stable saw area, is the desirable operating area.

This diagram summarizes the traditional critical speed theory and precisely applies to fixed-collar saw. However, for guided circular saws, experimental and industrial experiences [3, 4] suggest that there are not two distinct curves that divide the entire region into three areas. Instead of the critical speed instability, the interaction between workpiece and saw may be the key factor influencing guided saw cutting behavior. The tasks left to us will be the explanation of these experimental and industrial experiences by using the experimental method and the theory that we need to find.

3.0 Preliminary Experimental Study

This experimental study was motivated by some previous work [2, 3, 5, 21] on the cutting behaviors of fixed-collar and guided saws. As mentioned in the Introduction, the fundamental questions of interest are: how do guided saws work, and what are the most important saw design factors? The question of how closely guided saw behavior follows the traditional critical speed theory is the starting point of this experimental study. The sawing machine and the experimental set-up are introduced first. After that, the experimental work is described. This includes some initial tests with a fixed-collar saw, initial test results, the cutting test plan, wood cutting tests with a fixed-collar saw and a guided saw and their results. Finally a discussion of the test results is given.

3.1 Sawing Machine

All experiments were performed on the sawing machine located in Wood Machining Laboratory of the Department of Mechanical Engineering at UBC. This machine, shown in figure 3.1, consists of a circular saw, guides (for a guided saw) or a fixed-collar (for an unguided saw), a rotating shaft, a carriage, hydraulic system, power supply, main control panel, and water supply system and so on.
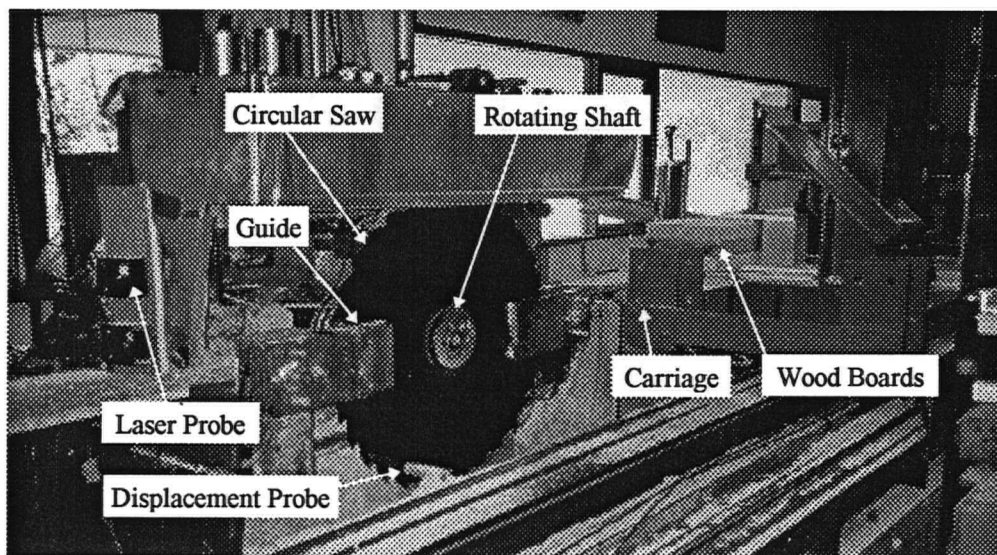
Figure 3.1: Sawing Machine

A hydraulic pump, driven by a 100 hp electric motor, can run the arbor from zero to 4000 rpm. A circular sawblade is driven by either a spline-arbor with a guide or a fixed-collar. In wood sawing, the wood boards, which are mounted on a carriage that is driven by another hydraulic pump, go through the rotating sawblade to complete an entire sawcut at various feed speeds from zero to 480 fpm. The main control panel is used to control the rotation speeds of the saw, the feed directions and the feed speeds of the carriage, the stoppage of the sawblade, the carriage or the entire machine, etc. A water supply system provides water for the guide and sawblade to serve as lubricant and coolant.

3.2 Experimental Set-up

Figure 3.2 and figure 3.3 schematically depict the experimental apparatus arrangements for the fixed-collar saw and the guided saw. The main specifications of the test saw are listed in figure 3.4. The feed speeds and feed per tooth of the fixed-collar and guided saws are shown in Appendix.
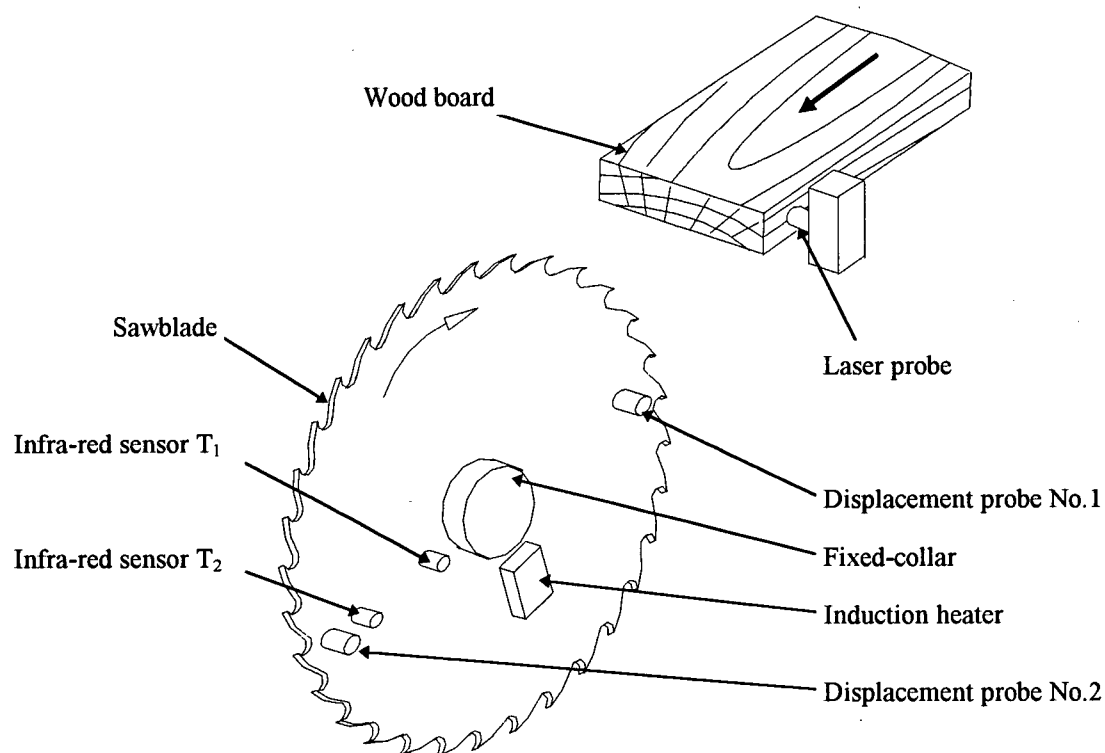
Figure 3.2: Schematic Arrangement of a Fixed-collar Saw Measurement

Wood boards

Displacement probe No.1

Sawblade

Displacement probe No.2

Top laser probe

Bottom laser probe

Guide

Spline-arbor

Induction heater

Infra-red sensor T_1

Infra-red sensor T_2
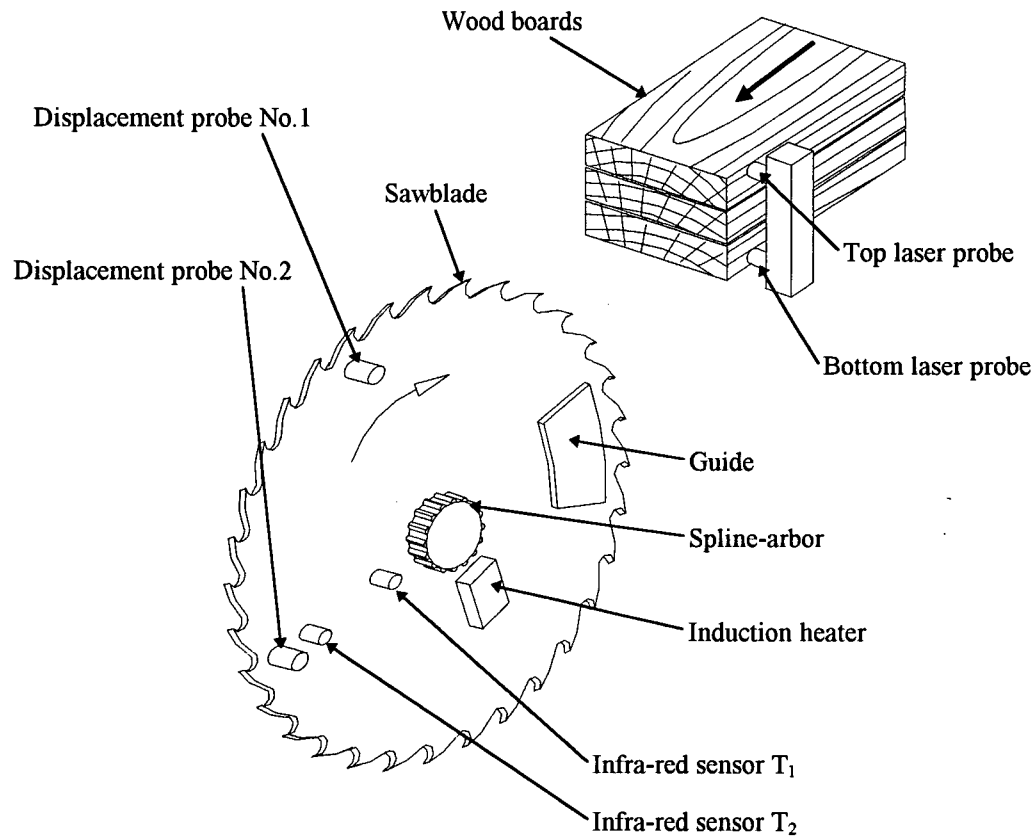
Figure 3.3: Schematic Arrangement of a Guided Saw Measurement

Saw parameter name	British unit		Metric unit	
Outer diameter	30	in	750	mm
Collar diameter	7	in	175	mm
Hole diameter	5.5	in	135	mm
Kerf width	0.103	in	2.5	mm
Plate thickness	0.075	in	1.9	mm
Gullet area	0.89	in^2	575	mm^2
Number of teeth	32		32	

Figure 3.4: Specifications of Test Saw

Two non-contact induction-type displacement probes measured the lateral displacements of the sawblade at the points indicated in figures 3.2 and 3.3. Figure 3.5 shows the electrical measurement equipment set-up.

The guide for the guided saw arrangement was installed in the position shown in figure 3.3. The clearance between the sawblade and the guide was between 0.07 mm and 0.13 mm. Water, used as lubricant and coolant, was introduced into the gap between the blade and the guide through holes in the guide.
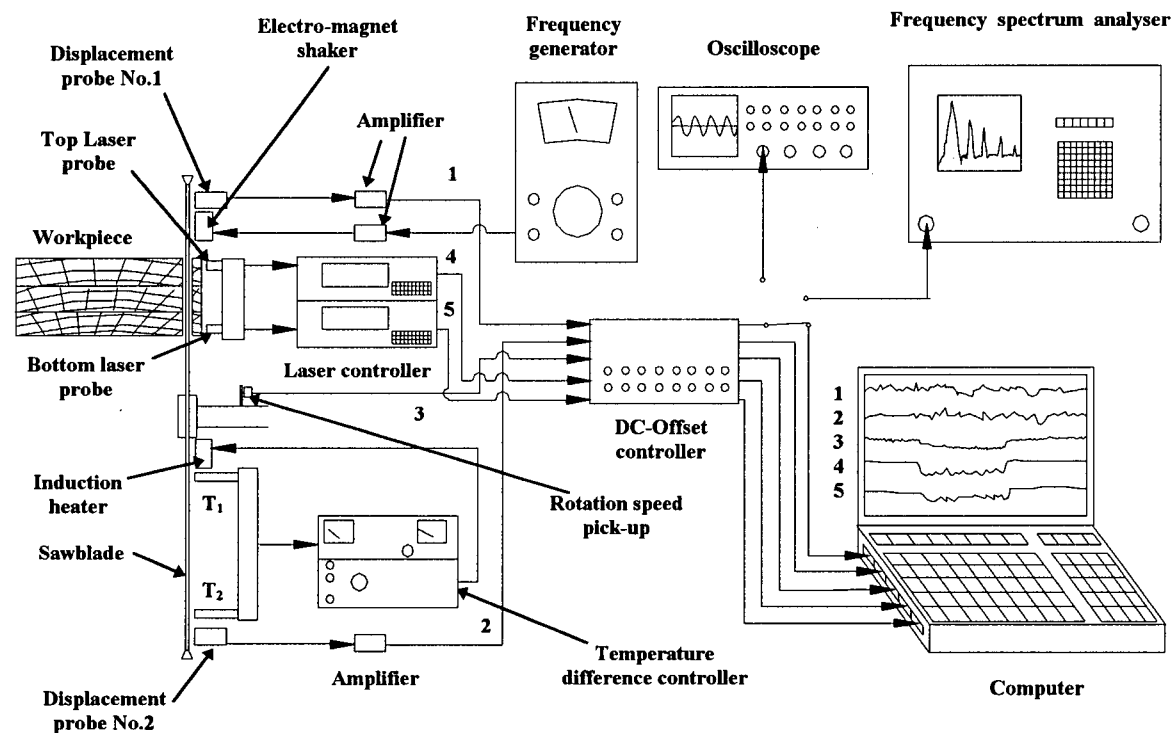
Figure 3.5: Electrical Measurement Equipment Set-up

In this experiment, temporary thermal tensioning, induced by non-uniform heating, was provided by a Jajod "Thermostress" system [2]. In this system, an induction heater was used to heat the central area of the sawblade. The temperatures of the inner area and outer rim of the sawblade, T_1 and T_2, were detected by two infra-red sensors. The intended temperature difference, $\Delta T = T_1 - T_2$, was automatically maintained by a control device. The non-uniform temperature along the radius of sawblade provided the needed temporary tensioning stresses for the saw. The maximum temperature difference

ΔT generally depended on the saw rotation speed and saw dishing. At high saw rotation speeds, the maximum temperature difference ΔT becomes limited because of the large convective heat loss from the rapidly rotating saw. In this experiment, the temperature difference ΔT was set in the range of $0°C$ - $12°C$. The maximum temperature reached at the central area of the saw was $42°C$, which is far below the temperature that causes any permanent effects.

After cutting, the workpiece was returned to its initial position and then run forward again. During the second motion of the workpiece, two Keyence laser displacement probes beside the sawblade measured the sawn surface profile along the length of the workpiece. The upper laser probe detected the board surface profile along the upper edge, corresponding to the outer rim of the saw. The lower laser probe detected the board surface profile along the lower edge, corresponding to the center area of the saw. In the case of the fixed-collar saw, only the lower probe was used.

In this experiment, according to different cutting capacities of the fixed-collar and guided saws, two types of green Hemlock boards with different dimensions were used as the test wood. In the fixed-collar saw tests, only one board 8 feet long × 10 inches wide × 1.5 inch high was cut each time. The saw could not successfully cut a greater depth of wood without excessive side-to-side deviation. In the guided saw tests, three boards, each one 8 feet long × 10 inches wide × 1.875 inches high, were cut each time. The guided saw was found to be able to cut a much greater depth of wood without excessive side-to-side deviations. Wood pieces around 0.25 inch thick were cut during each cutting stroke.

A computer was used to record all the signals from displacement probes, laser probes and rotation speed pick-up, as shown in figure 3.5.

In addition, in the initial tests, as shown in figure 3.5, an oscilloscope was used to detect dishing speeds of the saw caused by the thermal tensioning. A frequency spectrum analyzer also was used to measure the natural frequencies to find the critical speed of the

fixed-collar saw. An electro-magnet shaker was mounted close to the sawblade to excite sawblade vibration.

3.3 Experimental Work

Firstly, some initial tests were conducted to measure the dishing and critical speeds of the fixed-collar saw for the full range of thermal tensioning. After that, cutting tests with a fixed-collar saw were performed to examine how well the results of these tests followed expectations from the critical speed theory. Then an experiment was done with the guided saw to investigate how closely these results compare with the results from the fixed-collar saw.

3.3.1 Initial Tests

1. Measurements of Dishing Speeds of a Fixed-collar Saw

In the dishing speed tests with a fixed-collar saw, the rotation speeds were set from 750 rpm to 1830 rpm in 60 rpm intervals. The induction heater was slowly adjusted to provide increasing amounts of thermal tensioning, as represented by the temperature difference ΔT. The onset of dishing was identified by observing the signal from displacement probe No.1 on an oscilloscope. The corresponding saw rotation speed and temperature difference ΔT were recorded. A sudden position change of the electrical signal indicated a rapid motion to one side of the saw rim. In general, the required temperature difference increased with increasing the rotation speed. Figure 3.7 shows the measured relationship between the dishing speed and the amount of tensioning.

2. Natural Frequency Measurements of a Fixed-collar Saw

In the idling tests with a fixed-collar saw, the natural frequencies of the saw were measured over a range of rotation speeds and thermal tensioning. For each temperature difference ΔT from 0°C to 8°C in 2°C intervals, saw rotation speed was slowly adjusted from 0 to 2160 rpm in 60 rpm intervals (120 rpm intervals applied to the rotation speeds far away from critical speed). An electro-magnet shaker excited sawblade to produce a vibration signal that could be detected by the displacement probes. Then the spectral

content of the electrical signal from displacement probe No.1 was identified using a frequency spectrum analyzer. The lowest natural frequencies with the most prominent vibration amplitudes were recorded and plotted in a diagram to determine the lowest critical speed. Figure 3.6 shows an example diagram. The critical speed was determined to be the rotation speed when the lowest natural frequency equaled zero. For the temperature difference ΔT from 0°C to 8°C in 2°C intervals, a critical speed line was formed in the diagram of rotation speed vs. tensioning, as shown in figure 3.7.

3. Initial Test Results

Figure 3.6 shows a graph of the natural frequencies vs. rotation speed of the fixed-collar saw with no added tensioning $\Delta T = 0$. The forward traveling wave frequencies increase with increase in rotation speed and the backward traveling wave frequencies decrease with increase in rotation speed. The lowest critical speed was determined to be around 1530 rpm = 25.5Hz by selecting the rotation speed with the lowest natural frequency equal to zero.
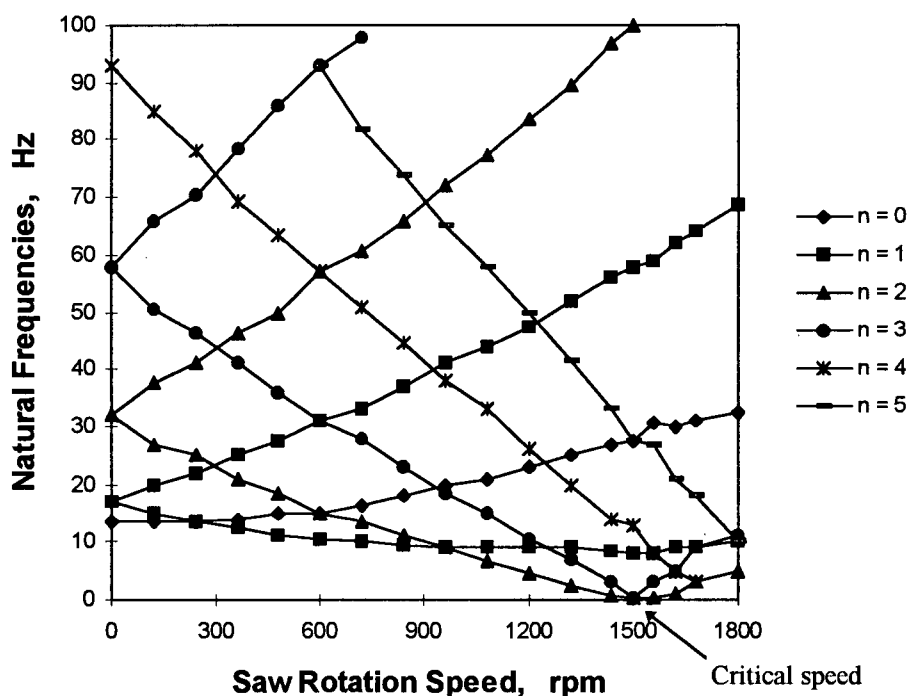
Figure 3.6: Natural Frequencies and Rotation Speed of a Fixed-collar Saw, No Added Tensioning $\Delta T = 0$

Similar diagrams (not shown) for thermal tensioning ΔT from 2°C to 8°C in 2°C intervals provided the other critical speeds.

Figure 3.7 summarizes the measured critical speeds and dishing speeds as a function of the amount of thermal tensioning. Because there was not enough power to increase the temperature difference ΔT further at higher rotation speeds, the maximum possible ΔT was 8°C in these measurements. The calculated critical speeds and dishing speeds of the fixed-collar saw [2] is also included as a comparative reference in the diagram.
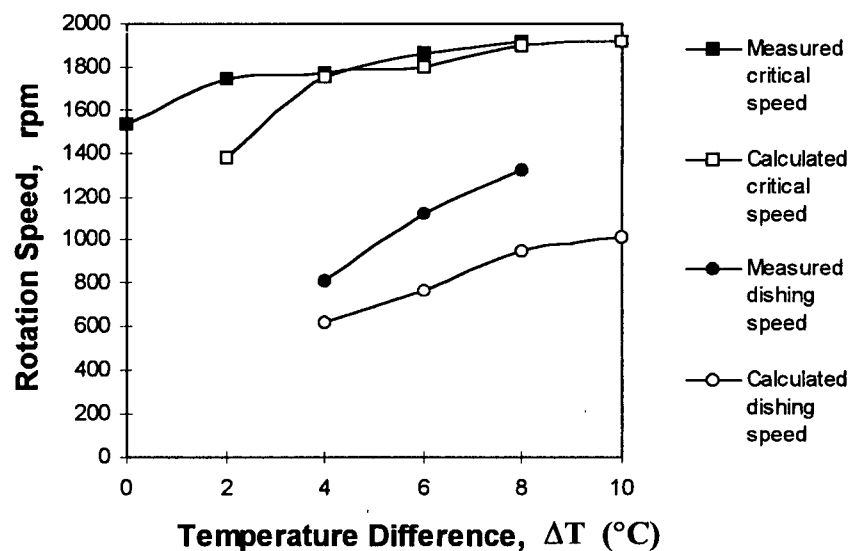
Figure 3.7: Critical and Dishing Speeds at Different Thermal Tensioning ΔT

Figure 3.7 shows that the measured critical and dishing speed lines generally follow the trends from the theoretical expectations. From the previous studies [2], the calculated critical speeds were slightly higher than the measured values and the calculated dishing speeds were slightly lower than the measured values.

3.3.2 Cutting Tests with a Fixed-collar Saw

1. Cutting Test Plan

Cutting tests with a fixed-collar saw were performed to determine how well the behavior of a fixed-collar saw follows the traditional critical speed theory. In the tests, only one

board 8 feet long × 10 inches wide × 1.5 inches high could be cut without overloading the saw. Cutting tests were done for all combinations of rotation speed from 800 rpm to 1800 rpm in 200 rpm intervals (6 speeds), and thermal tensioning settings ΔT from 0°C to 10°C in 2°C intervals (6 settings). This constituted 6 × 6 = 36 combinations. Measurement of each combination was repeated four times. The sequence of experimental measurements was randomized so as to reduce any systematic effects due to natural differences in the wood boards and wear of the saw teeth. In total, 144 cuts were done using 12 workpieces.

In the cutting tests, the feed per tooth of each rotation speed was adjusted to be constant. The gullet feed index was maintained at 0.09 because of the lower cutting capacity of this large and thin fixed-collar saw through several initial trials. Following formulae represent the relationship of the cutting parameters.

$$\text{gullet feed index} = \frac{\text{feed per tooth} \times \text{cutting height}}{\text{tooth gullet area}} \qquad (3.1)$$

$$\text{feed per tooth} = \frac{\text{feed speed}}{\text{saw rotation speed} \times \text{number of teeth}} \qquad (3.2)$$

Before the tests, all feed speeds of the corresponding rotation speeds were adjusted to the specified values in advance. The feed speeds and feed per tooth of a fixed-collar saw are shown in Appendix. After cutting, the sawn surface profile was measured by using the bottom laser probe and the computer, as shown in figure 3.5. The vibration signals from all the displacement probes were also recorded by the computer. Then the standard deviations of the surface profile were calculated from the average of the four sets of repeat measurements. These standard deviations represent cutting accuracy. Finally, the standard deviations over the range of the rotation speeds and saw tensioning was plotted in a contour line diagram to show the relationship of cutting accuracy to rotation speed and saw tensioning.

2. Cutting Test Results

Figure 3.8(a) depicts an example measurement of saw lateral vibration displacement at probe 1 vs. elapsed time. The temperature difference ΔT was 2°C and the rotation speed was 1600 rpm for this particular test. Figure 3.8(b) depicts the sawn surface profile vs. the board length corresponding to figure 3.8(a), measured by using the laser probe on the stroke after cutting shown in figure 3.2. The abscissae of two curves have been adjusted to make the time position correspond to the board length. The trends of figure 3.8(a) and figure 3.8(b) are very similar. The same behavior was observed in almost all measurement. This confirms that the saw vibration directly controls the cutting accuracy.
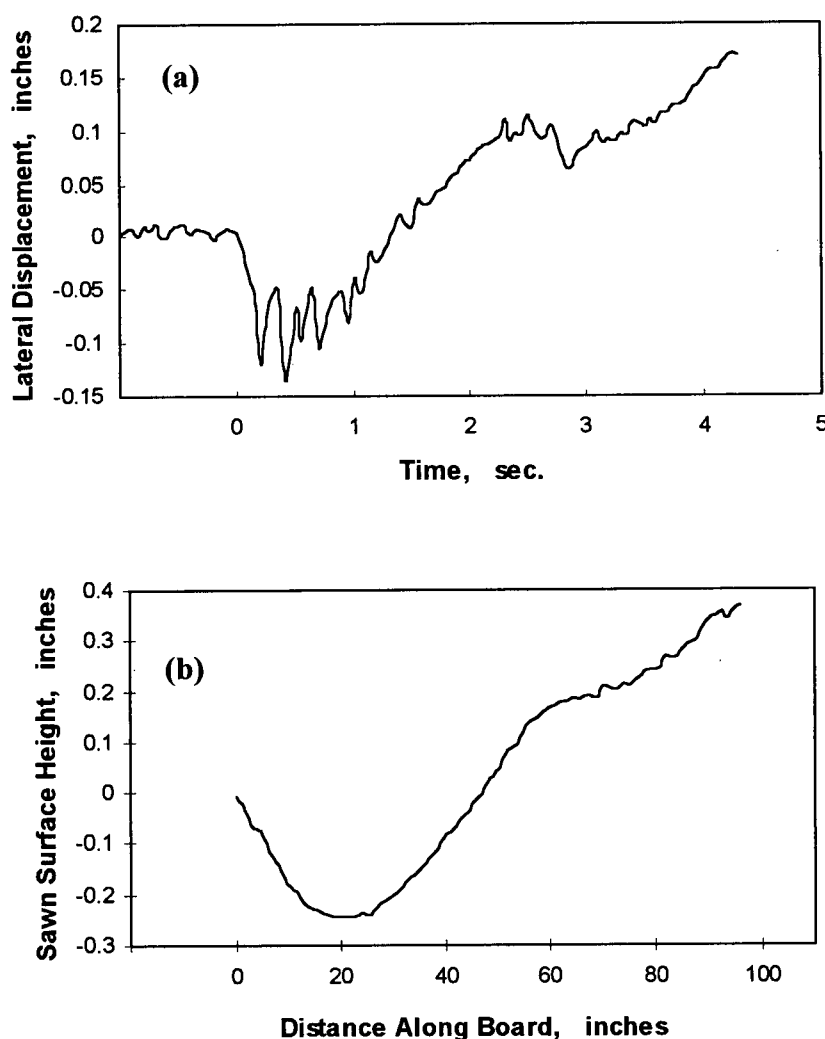
Figure 3.8: (a) Saw Lateral Vibration; (b) Workpiece Surface Profile. Rotation Speed = 1600 rpm, ΔT = 2°C, Gullet Feed Index = 0.09, and Cutting Depth = 1.5 inch.
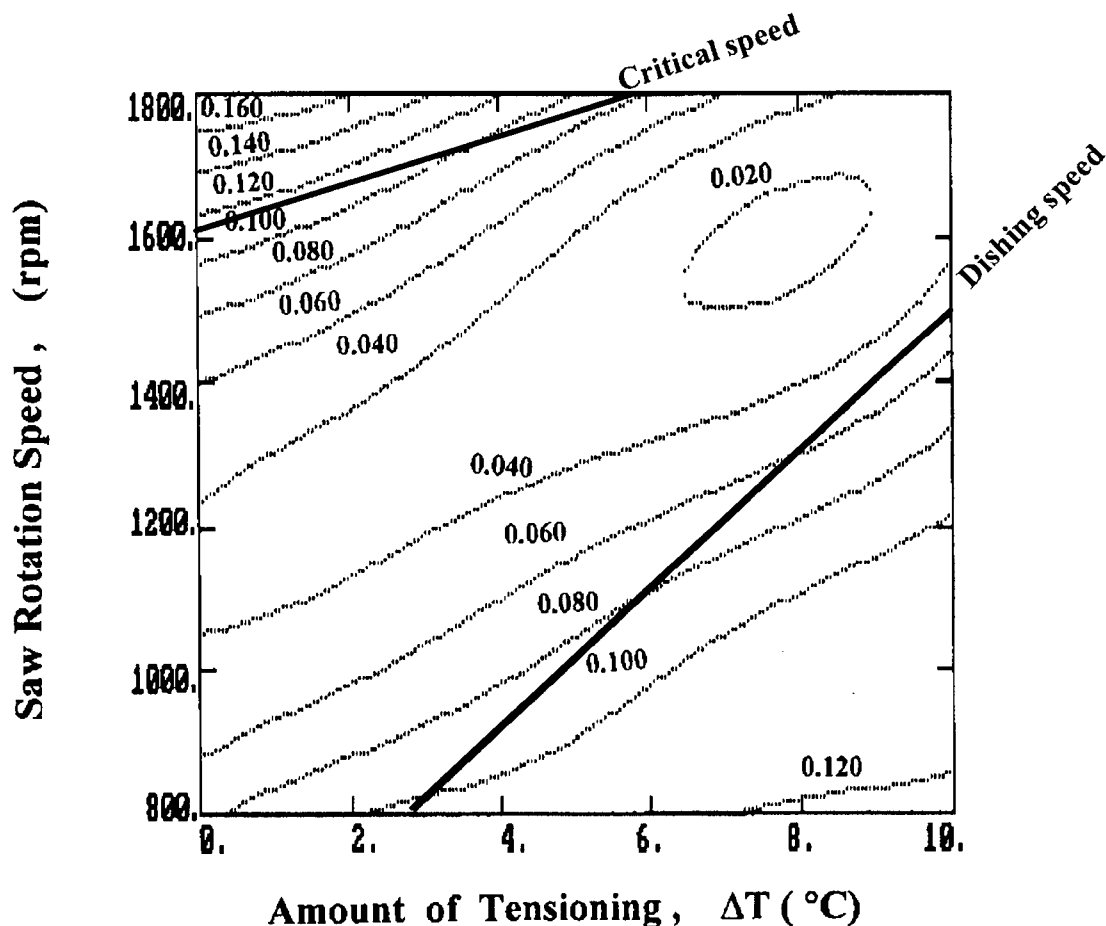
Figure 3.9: Sawcut Standard Deviation for a Fixed-collar Saw over a Range of Rotation Speeds and Tensioning States

The wood sawing accuracy is represented by the sawcut standard deviation of the sawn surface profile over the lengths of the boards. Zero sawcut standard deviation represents a perfectly straight sawn surface. Higher sawcut standard deviations represent progressively poorer wood sawing accuracy. Figure 3.9 shows a contour plot of the standard deviations of the sawcuts, measured over the range of rotation speeds and temperature difference ΔT that were tested. In this diagram, each line represents a specified sawcut standard deviation, namely cutting accuracy. The contour line diagram figuratively depicts the cutting accuracy changes over the tested range.

In figure 3.9, the sawing accuracy change profile is like a valley. In the lowest point of the valley, within the 0.020" contour the most accurate sawing is achieved. A maximum standard deviation value of 0.16 inches is obtained at upper left corner. The corresponding maximum value of 0.12 inches is at the lower right corner for a dished saw. Because the cutting area was out rim of the sawblade where larger lateral vibration amplitude occurred, the large standard deviation values were caused in the extreme cases. Along both sides of the valley, corresponding to the snaking saw and dished saw areas in figure 2.3, much inferior sawing accuracy occurs. The critical speed and dishing speed lines lie approximately parallel to the valley, on either side of the minimum area. The tendency of the standard deviation in figure 3.9 follows the expectations from figure 2.3. The best cutting accuracy (lowest standard deviation) occurs between the critical speed and dishing lines. The cutting accuracy deteriorates rapidly in both areas beyond the two lines.

3.3.3 Cutting Tests with a Guided Saw

1. Cutting Test Plan

In these cutting tests, three boards of 8 feet long and combined height of 5.625 inches were cut to compare the behavior of the guided saw with that of the fixed-collar saw. The tests followed a similar sequence of saw cutting conditions as was used with the fixed-collar saw. Tests were done for all combinations of rotation speed in the range 800 rpm to 1800 rpm in 200 rpm intervals, and thermal tensioning settings ΔT from 0°C to 12°C in 2°C intervals. Each combination of rotation speed and thermal tensioning setting was performed three times. Also the tests with the same rotation speed were conducted in three different boards. As before, this sequence was used to randomize the cutting sequence to avoid bias due to tool wear, individual workpiece characteristics, etc. In total, 126 cuts were done by using 27 workpieces.

In the tests, the feed per tooth at each rotation speed was adjusted to maintain a constant value. The gullet feed index was maintained at 0.25, much higher than was possible with

the fixed-collar saw. The feed speeds and feed per tooth of a guided saw are shown in Appendix.

The other descriptions of the tests were the same as for the fixed-collar saw tests. Finally the contour line diagram was formed to show the relationship of cutting accuracy to rotation speed and saw tensioning. The results from three repeated cutting tests at each cutting condition were averaged to improve accuracy.

2. *Cutting Test Results*

Figure 3.10 shows the standard deviations of the sawcuts, measured over the entire range of rotation speeds and temperature differences ΔT, and plotted in the contour line diagram. In this diagram, each line represents a specified sawcut standard deviation.
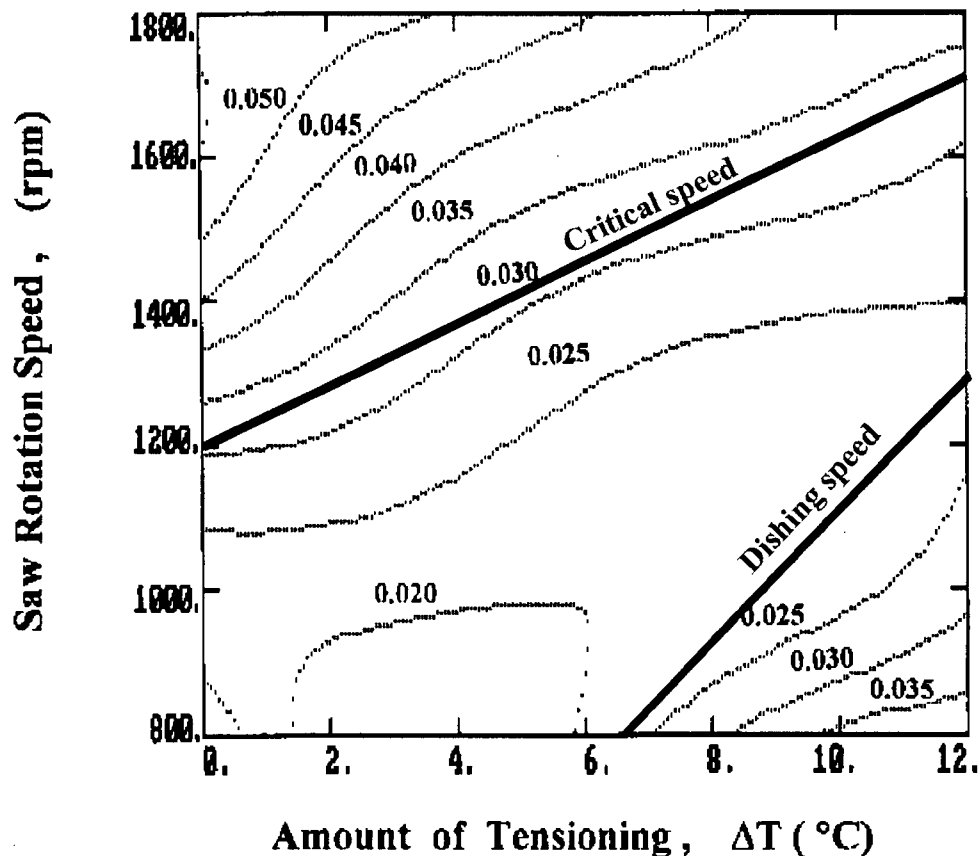
Figure 3.10: Sawcut Standard Deviation for a Guided Saw over a Range of Rotation Speeds and Tensioning States

The tendency of the cutting behavior illustrated in figure 3.10 is similar to that shown in figure 2.3.

Compared with figure 3.9, the critical speed and dishing speed lines drop somewhat. This conforms to the previous study result [15] that a guided saw has the same or lower critical speed as that of a fixed-collar saw of the same dimensions.

In figure 3.9, the standard deviation of the fixed-collar saw changes from a minimum value of 0.02 inches to a maximum value of 0.16 inches at upper left corner. This is an increase of 700%. The corresponding change at the lower right corner is from 0.02 inches to 0.12 inches, an increase of 500%. This shows that the critical speed and dishing speed areas make the sawing quality deteriorate rapidly for a fixed-collar saw.

In figure 3.10, the standard deviation of the guided saw changes from a minimum value of 0.02 inches to a maximum value of 0.05 inches at upper left corner. This is an increase of 150%. The corresponding change at the lower right corner is from 0.02 inches to 0.035 inches, an increase of 75%. This shows that the critical speed and dishing speed areas make the sawing quality deteriorate much less rapidly for a guided saw.

The standard deviation of figure 3.10 is much smaller than the one of figure 3.9 in the critical speed and dishing speed areas. Both of them have the same minimum standard deviation of 0.02 inches in the middle area. The maximum standard deviation of 0.16 inches for critical speed area in figure 3.9 is 3.2 times larger than the one in figure 3.10. For dishing speed area, the maximum value of 0.12 inches in figure 3.9 is 3.4 times larger than the one in figure 3.10.

The much greater cutting capacity of the guided saw is confirmed by the following comparisons:

- The cutting depth of 5.625 inches for the guided saw was 3.75 times thicker than the 1.5 inch cutting depth of the fixed-collar saw.

- The gullet feed index of 0.25 for the guided saw was 2.8 times larger than the 0.09 value for the fixed-collar saw.

The general pattern of the guided saw cutting accuracy is similar to that of the fixed-collar saw in figure 3.9. However, there are no obvious critical speed and dishing speed lines to divide figure 3.10 into three areas as in figure 3.9. The operating speeds of the guided saw, close to or above the critical speed line, still produced fairly stable cutting. The guided saw had a wider range of acceptable cutting accuracy. The standard deviations of the guided saw were also relatively insensitive to tensioning. Therefore, compared with the behavior of the fixed-collar saw which closely matches the traditional critical speed theory, the behavior of the guided saw only weakly follows theoretical expectation from the traditional critical speed theory.

3.4 Discussion

The purpose of these preliminary experimental studies was to investigate the fundamental questions by doing comparative tests to determine how closely guided saw behavior compares with the expectations from the traditional critical speed theory. The experimental results clearly indicate that the behavior of a guided saw only weakly follows the theoretical expectation from the traditional critical speed theory.

The experimental observations also provides the following insights to investigate the fundamental questions:

- Figure 3.8(a) shows that the fixed-collar saw became unstable during cutting while it was stable while idling. This figure was a typical diagram in the experimental data recording. There may exist some reactions between workpiece and saw.

- At the start of the fixed-collar saw tests, during a light cut the sawblade dived to one side, overheated, became permanently bent and finally stopped. This happened with a workpiece feed speed much lower than the speeds that were

easily handled by the same sawblade with a guide. This phenomenon suggested an important interaction between workpiece and saw body.

- The comparisons between the guided saw results and the fixed-collar saw results clearly show the difference of their cutting behaviors. Guided saws definitely have superior cutting accuracy and can cut wood stably close to and above critical speed line. Guided saws only partly follow the traditional critical speed theory.

Industrial and experimental experience [4] suggests that guided saws can be stably operated at supercritical speeds. This conforms to the results of the current experiment.

The previous experimental studies [3] indicate that the behavior of an idling guided saw closely follows the expectations of traditional critical speed theory. In current experimental studies, a cutting guided saw weakly follows the traditional critical speed theory. It is obvious that during cutting the interaction between workpiece and saw makes the idling guided saw lose part of the behavior consistent with traditional critical speed theory.

From the present experimental results and observations, and also industrial and previous experimental experiences, the interaction between workpiece and saw is identified as an important factor that controls how guided saws work. This important factor still needs further studies to give more detailed understanding.

4.0 Saw-Workpiece Interactions

In this chapter, a hypothesis is presented concerning the interaction between the saw and the workpiece. Two aspects of saw-workpiece interaction are investigated. They are the interaction between the saw body and the workpiece, and between the saw teeth and the workpiece. The proposed geometrical interaction mechanisms are based on experimental observations. The objective is to investigate the physical meaning of the interaction so as to understand its significance for wood cutting using circular saws.

4.1 Hypothesis

In preliminary experimental studies, significant interactions between the saw and workpiece were observed. The experimental results strongly suggest that an important factor controlling guided saw cutting behavior is the interaction between the workpiece and saw.

Two aspects of the interaction include the interaction between the saw body and the workpiece and the one between the saw teeth and the workpiece. These interactions are described in the following paragraphs.

4.2 Saw Body-Workpiece Interaction

As mentioned in the Introduction, modern industrial saws are designed to be as thin as possible to increase lumber recovery. However, thin sawblades are very flexible. When heavily loaded, such sawblades can easily be bent to one side by cutting forces. Figure 4.1 shows a plan view of a fixed-collar saw. In the diagram, the fixed-collar saw has been bent to one side during wood sawing. The sideways displacement of the sawblade exceeds the side clearance of the teeth. When continuing to go forward further, the workpiece will touch the side surface of the sawblade at point S. This point is upstream of the sawblade support provided by the fixed-collar. Therefore, further advance of the workpiece makes the contact point S move forward and bend the sawblade more. This results in a runaway sideways veering of the sawcut. In severe cases, the sawblade

overheats due to large contact friction and fails dramatically. Such a failure was observed in a preliminary experiment with a fixed-collar saw.
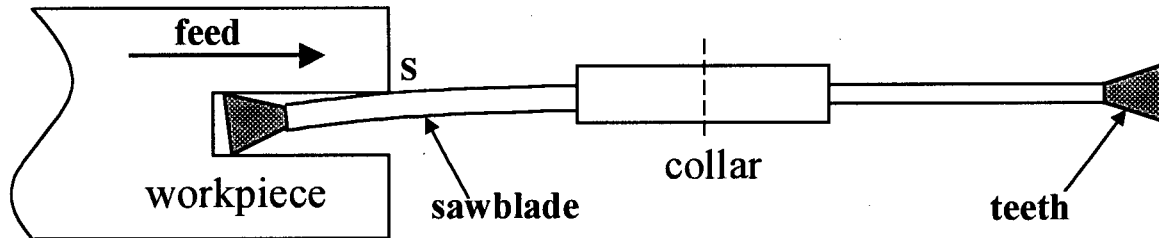
Figure 4.1: Plan View of a Fixed-collar Saw Bent to One Side due to the Interaction of the Saw Body with the Workpiece

The behavior shown in figure 4.1 can be further understood by considering an analogy. Figure 4.2 shows an analogous diagram of a boat moored in a river with its rudder pointing upstream. In this diagram, the flowing water, the rudder and the boat respectively correspond to the workpiece, the sawblade and the fixed-collar in figure 4.1. The rudder, representing the sawblade, is upstream of the boat. When the rudder (sawblade) inclines to one side due to a lateral force, the flowing water, representing the workpiece, makes it veer far to that side.
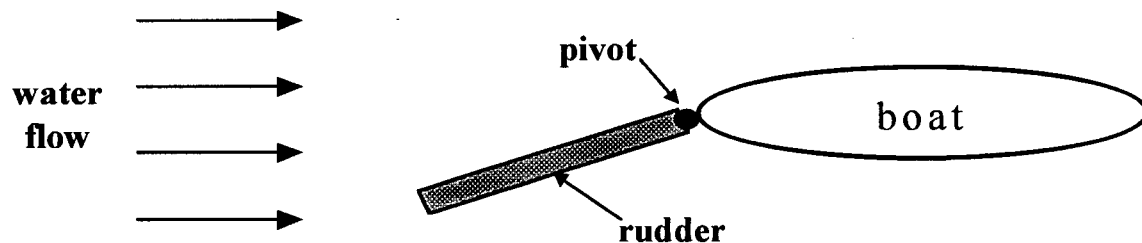
Figure 4.2: Rudder Analogy : A Boat Moored in a River with Its Rudder Pointing Upstream

A guided saw shows a different behavior during wood cutting. Figure 4.3 shows a plan view of a guided saw. In this diagram, the guided saw has been bent to one side and contacts the workpiece at point T. However, in this case, the contact area is downstream of the sawblade support represented by the guides. Therefore, when continuing to

advance, the workpiece pushes the sawblade back in line. In practice, a similar behavior almost always happens with a guided saw. The teeth at the outfeed end run along the previously sawn surface, and make that part of the sawblade follow the sawcut line.
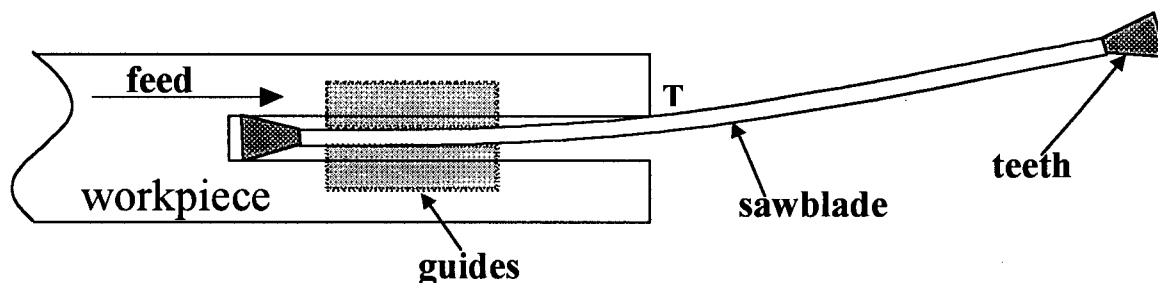
Figure 4.3: Plan View of a Bent Guided Saw Pushed in Line due to the Interaction of Saw Body with Workpiece

The above mentioned behavior of a guided saw can also be understood by using a rudder analogy. Contrary to the situation of figure 4.2, the arrangement of this analogy shown in figure 4.4 places the rudder on the downstream end of the boat. In this diagram, the flowing water, the rudder and the boat respectively represent the workpiece, the sawblade and the guides in figure 4.3. The rudder, acting as the sawblade, is downstream of the boat, corresponding to the guides in figure 4.3. If the rudder (sawblade) inclines to one side, the flowing water (workpiece) pushes the rudder back in line.
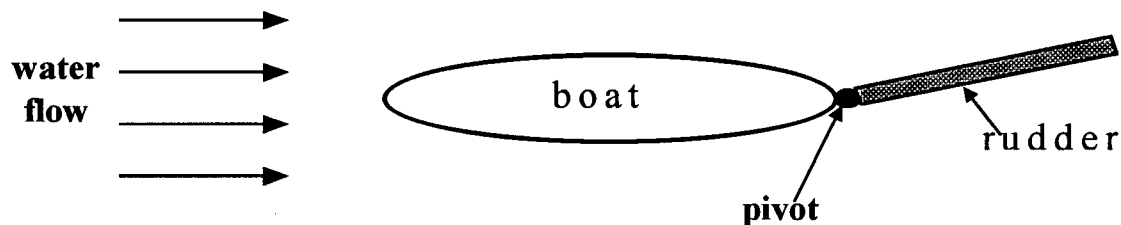
Figure 4.4: Rudder Analogy: A Boat Moored in a River with Its Rudder Pointing Downstream

This viewpoint can also give a possible explanation of why spline-arbor saws can provide more accurate sawcuts than can floating-collar saws. Both spline-arbor saws and floating-collar saws have guides to provide support and increased stiffness near the cutting area.

From the point of view of the traditional critical speed theory, for a floating-collar saw, the additional support and stiffness provided by the collar make it have a higher critical speed than a spline-arbor saw of the same size. Therefore, it might be expected that a floating-collar saw would have a further advantage. However, this is not the case. This is because the increased body stiffness may inhibit the self-centering behavior illustrated in figure 4.3 and figure 4.4. In contrast, a more flexible spline-arbor saw with the lower stiffness and critical speed provides more accurate results. The combination of a stiff cutting zone and a flexible body appears to be an advantageous choice. It works well particularly for curve sawing applications. Although more body flexibility is not the only reason for preferring spline-arbor saws, at least it can give a support to understanding how the interaction between the saw body and workpiece influences guided saw cutting behavior.

Industrial experience gives some support to this rudder analogy of guided saw-workpiece interaction. Compared with using only infeed guides, using guides at both infeed and outfeed ends have shown inferior cutting performance. This is different from what might be expected from the increased saw stiffness. This guided saw behavior is usually explained by the misalignments that exist between the infeed and outfeed guides. However, these two side guides can easily be aligned to tolerances much smaller than the saw runout, and therefore the above mentioned explanation is open to question. Another possible reason is that the outfeed guides limit the rudder motion of the saw, and weakens the stabilizing effect of the infeed guides.

4.3 Saw Tooth -Workpiece Interaction

The interaction mentioned above involves lateral forces applied to the saw body by the workpiece. The other possible interaction involves cutting forces in the feed direction acting on the saw teeth. Figure 4.5(a) shows a plan view of a fixed-collar saw bent to one side during wood sawing. As shown in figure 4.5(b), this situation is counter-cutting. The tooth movement direction is opposite to the direction of the workpiece. This is the traditional arrangement because it is inherently safe. In this situation, workpiece tends to

be pushed out of the cut by the saw, and therefore any small slippage in the wood transport system does not have serious consequences.

In the counter-cutting shown in figure 4.5, the advancing workpiece applies a compressive radial force on the saw. This force combines with the lateral displacement shown in figure 4.5(a) to create an additional moment load that further bends the sawblade. When the force is sufficiently large, the sawblade bending moment continuously increases and finally the sawblade buckles [23].
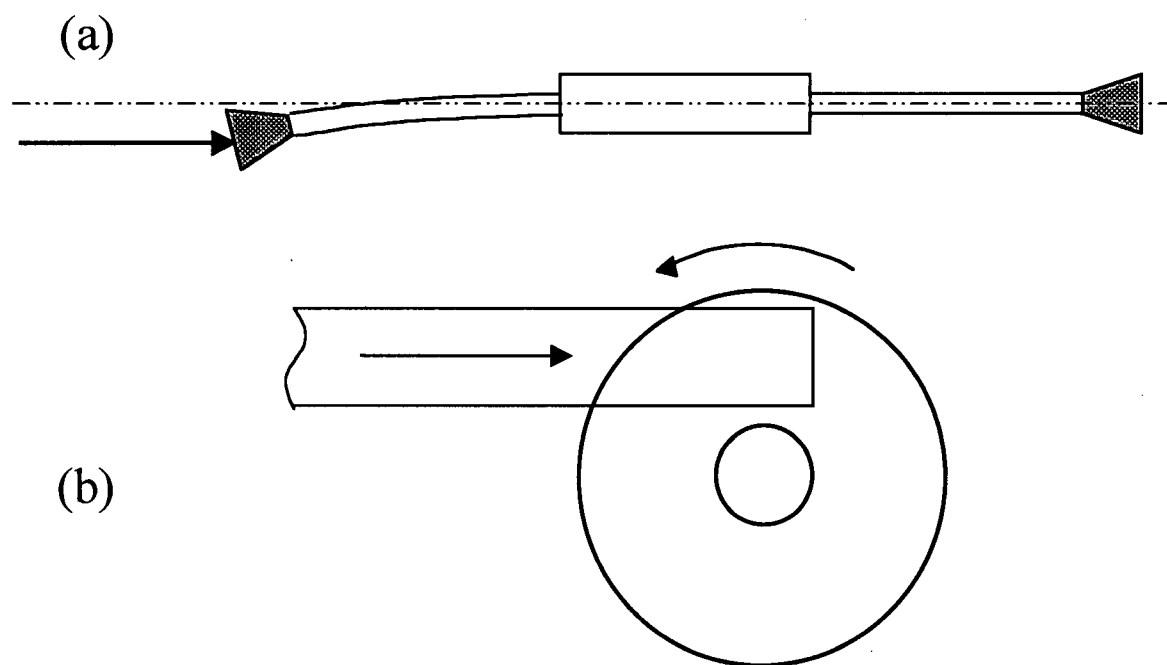
Figure 4.5: Feed Forces Force on a Fixed-Collar Saw, (a) Plan View, (b) Side View

For a counter-cutting guided saw, the feed forces also create a compressive radial force, and therefore saw buckling is also possible if the compressive force is high enough. However, guided saws typically have larger resistance to buckling than fixed-collar saws. The reason is that the guides support the sawblade much closer to the cutting area than the fixed-collar does. Figure 4.6 shows the comparison of how close to the cutting area

the guides and fixed-collar are. It is clear that d_2 is larger than d_1. Experience shows that cutting with the guides closer to the cutting area produces more stable sawcuts.
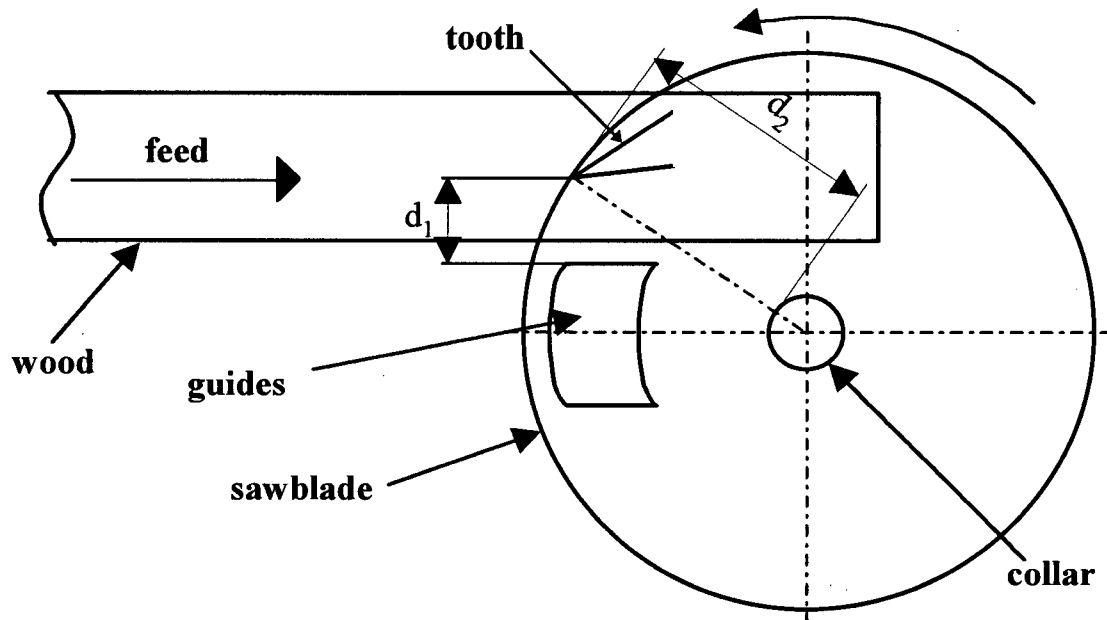
Figure 4.6: Comparison of the Distances Between Cutting Area and Support (Guides or Fixed-collar), $d_2 > d_1$

Compared with counter-cutting saws, climb-cutting saws cut wood in the reverse rotation direction. The tooth motion direction coincides with the feed direction in the cutting area [24]. This situation is not inherently safe. During wood cutting, the workpiece must be held very securely on the carriage to prevent it from being pulled into the saw and then thrown at high speed out the back of the machine.

Climb-cutting saws have an advantage in use. They typically cut more accurately than similar counter-cutting saws. Therefore, most new gangsaw machines installed in North American sawmills use climb-cutting saws. The deformed saw in figure 4.5 suggests a possible reason for the superior cutting accuracy of climb-cutting saws. Because the tooth motion direction in the cutting area coincides with the feed direction during climb-cutting, the cutting teeth tend to drag the workpiece forward. This reverses the sign of the radial force from that shown in figure 4.5(a) so that it becomes tensile. As a result, the feed force combines with the saw bending to produce a moment that reduces the saw

deformation. Sawblade buckling of the type occurring in figure 4.5(a) is then no longer a possibility. This is true for both fixed-collar and guided climb-cutting saws. However, the "rudder" type instability shown in figures 4.1 to 4.4 is almost uninfluenced by saw rotation direction except that the additional moment of climb-cutting reduces some amount of lateral displacement when the "rudder" action happens. Therefore, climb-cutting fixed-collar saws remain susceptible to the "rudder" effect, and superior cutting accuracy is still expected from guided saws during climb-cutting.

For climb-cutting, saw performance relies on many other different factors, not just those discussed here. Another explanation for the superior cutting accuracy of a climb-cutting guided saw is that the cutting area is the position where the sawblade has just left the guide. As a result, the guide freshly controls the sideways position at the cutting area and gives sideways deviations less chance to build up [25]. From another view, the sawdust that climb-cutting guided saws produce is carried away from the guides, and therefore the possibility of guides becoming blocked is greatly reduced. It is difficult to separate the factors described above from all the possible existing factors to determine which of them is the most important one influencing guided saw cutting behavior.

Table 4.1 summarizes the expected influences of the above-mentioned saw-workpiece interactions on the cutting stability of different saw types. Saw body-workpiece interaction exerts influences on the cutting stabilities of fixed-collar and guided saws. By comparison of each row in this table, the cutting stability of a guided saw is the superior selection. Saw tooth-workpiece interaction has influences on the cutting stabilities of counter-cutting and climb-cutting saws. By comparison of each column, the cutting stability of a climb-cutting saw is the superior selection. Therefore, from this comparative table, the cutting stability of a guided climb-cutting saw is expected to be best, while the cutting stability of a fixed-collar counter-cutting saw is comparatively poor.

		Saw Body - Workpiece Interaction	
		Fixed-Collar Saw	Guided Saw
Saw Tooth - Workpiece Interaction	Counter-Cutting Saw	Worst	Medium
	Climb-Cutting Saw	Medium	Best

Table 4.1: Comparison of the Cutting Stabilities of Different Saw Types Influenced by Two Saw-Workpiece Interactions

From the analyses of the two saw-workpiece interactions, the proposed hypotheses are plausible. The experiments done in this study are designed to provide further insight into these two saw-workpiece interaction mechanisms.

5.0 Saw-Workpiece Interaction Experiments

In this chapter, extensive experiments are described in which the two saw-workpiece interaction mechanisms previously described are examined. These experiments include some initial idling tests using a guided saw and extensive comparative cutting tests using the same saw with various guide configurations. The experimental preparation is first introduced, and then the experimental work is described. The description includes some initial tests with a guided saw, initial test results, the cutting test plan, the wood cutting tests with guided saws and their results. Finally a discussion is presented.

5.1 Experimental Preparation

All experiments in this chapter were conducted on the same sawing machine as was used in preliminary experimental study. The sawing machine is shown in figure 3.1.

Figure 5.1 schematically depicts the experimental equipment arrangement for the guided saw in the saw-workpiece interaction experiments. The sawblade used in the current experiments was the same as the one used in the preliminary experimental study. The specifications of the test saw are listed in figure 3.4.

Figure 5.1 shows the experimental set-up that was used. This set-up was similar to that used previously, shown in figures 3.2 and 3.3. The electrical measurement equipment shown in figure 3.5 applies to the arrangement shown in figure 5.1 except that figure 5.1 has two more displacement probes. The main difference is the guide arrangement. Two small guides were mounted at one side of the saw and one larger guide was mounted on the other side. These guides could be installed or removed so as to achieve several different guide configurations. In the present experiments, the installation, adjustment and operation procedures for the experimental apparatus are the same as for the preliminary experiments.

In the experiments, three Hemlock boards with each 8 feet long × 10 inches wide × 1.875 inches high were cut. Wood pieces around 0.25 inch thick were cut during each cutting stroke.
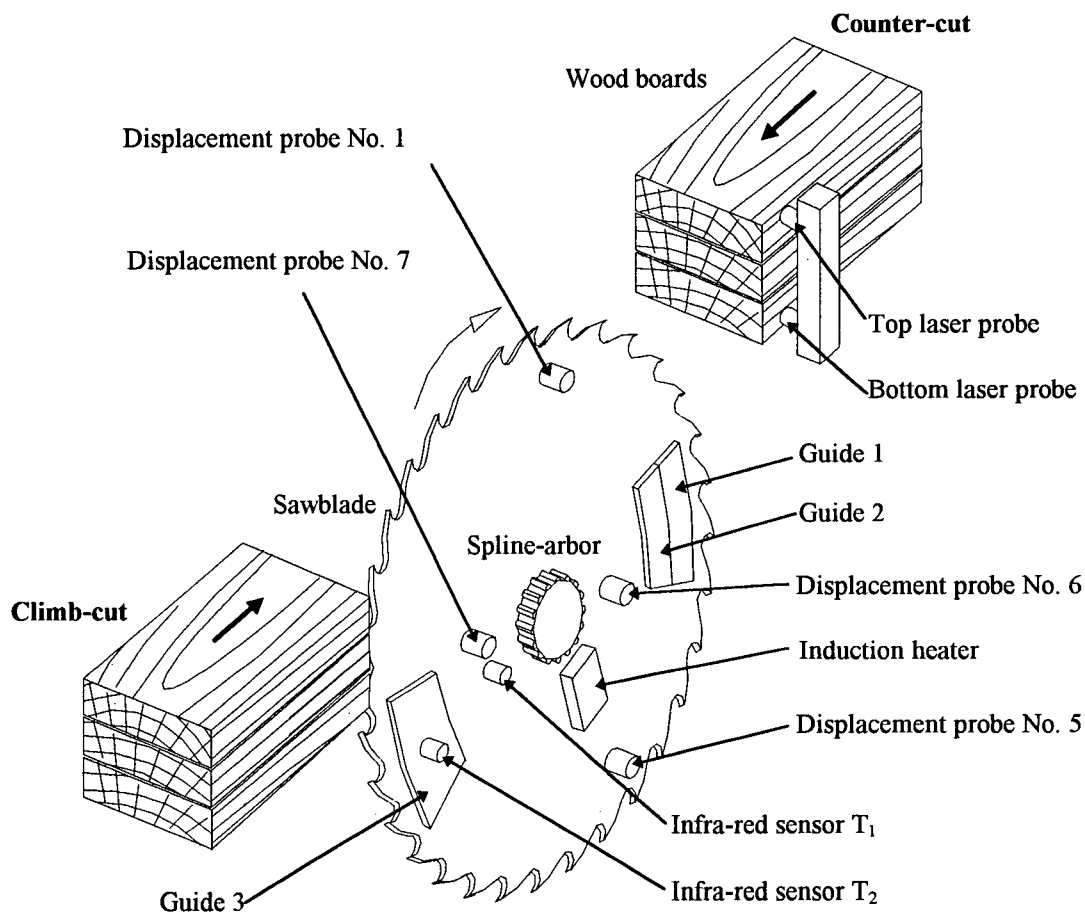
Figure 5.1: Arrangement of a Guided Saw Measurement

5.2 Experimental Work

5.2.1 Initial Tests

1. *Measurements of Dishing Speeds of a Guided Saw*

Firstly, some idling tests were performed to measure the dishing speeds of the guided saw using displacement probe No. 1, as shown in figure 5.1. The procedure was the same as was used in the preliminary experimental study. The rotation speeds were set from 120

rpm to 1380 rpm in 60 rpm intervals. A dishing speed line was plotted in a diagram of rotation speed vs. tensioning.

2. *Measurements of Temperature Profiles of a Guided Saw*

Satisfactory natural frequency measurements with the guided saw could not be achieved because of the large vibration signals caused by saw runout. Instead, the critical speeds of the guided saw have to be calculated from the measured saw temperature profiles. Therefore, in some idling tests, the saw temperature profiles were measured along the radius of the sawblade using a thermocouple. The range of the thermal tensioning was set from 2°C to 12°C in 2°C intervals and the rotation speed was 1200 rpm. The temperature profile was manually measured from center to outside within 30 seconds after stopping the saw. This sequence allowed the higher temperature region to be measured first because this region cooled more quickly.

3. *Measurements of Natural Frequencies of a Stationary Saw*

Natural frequency measurements of a stationary saw were performed by using a microphone and a vibration frequency spectrum analyzer. The measured natural frequencies of the stationary saw were compared with the calculated values in order to examine whether the original behavior of the saw was the same as the theoretical expectations.

4. *Initial Test Results*

Figure 5.2 shows the measured temperature profiles along a saw radius. This diagram clearly shows the area heated by the induction heater. The maximum measured temperature was 26°C, which is too low to produce any permanent effect on the saw.
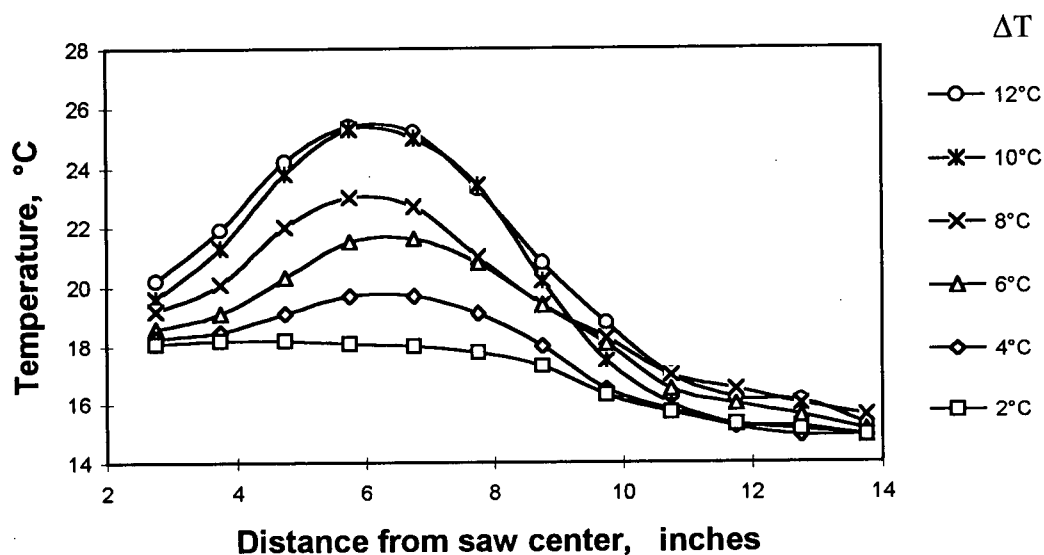
Figure 5.2: Temperature Profiles at Various ΔT

The measured temperature differences between the center and outer rim areas of the sawblade were generally less than the indicated ΔT value indicated by the Thermostress control unit. One of the reasons is that significant cooling occurred during the time required to complete the temperature measurements. Another reason is that the water from the guides distorted the working of the infra-red temperature sensors in the Thermostress unit.

An attempt was made to determine the critical speed of the guided saw using the same method as was used with the fixed-collar saw. This did not prove successful because of the substantial vibrational noise created by the interaction of the sawblade runout (lack of flatness) and the guides. Instead the saw critical speed was determined by calculation based on the measured temperature profiles in figure 5.2. To account for the cooling effects during temperature profile measurements, it was assumed that the temperature gradients were about 50% higher than indicated. Figure 5.3 shows the calculated critical speed and dishing speed curves corresponding to the temperature profiles in figure 5.2.
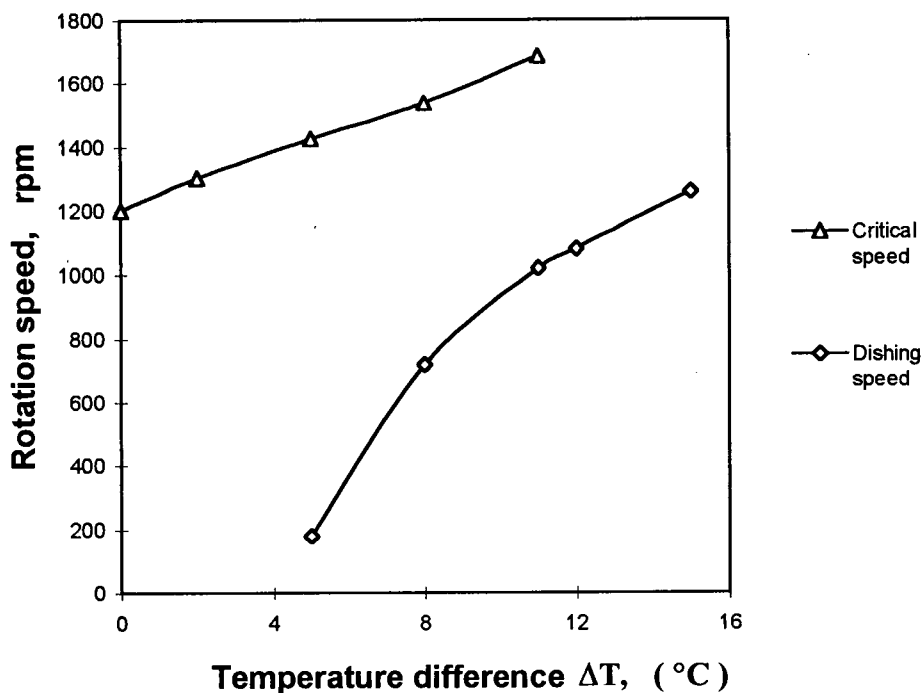
Figure 5.3: Critical and Dishing Speeds at Different Thermal Tensioning ΔT

5.2.2 Cutting Tests with Guided Saws

1. Cutting Test Plan

Extensive comparative wood cutting tests with various guide configurations were performed to examine the two saw-workpiece interaction mechanisms described in Chapter 4. Figure 5.4 shows a schematic of the various guide configurations and different feed directions used for the present experimental work.

In figure 5.4, the attachment method of the three guides was arranged so that each of them could easily be installed or removed. This arrangement allowed several guide configurations to be examined easily. They were guide 1 only, guide 1 + 2, guide 1 + 2 + 3 and guide 3 only. Guide 1 and guide 2 were smaller. They were located on the left of the sawblade. Guide 3 was larger and located on the right. The two smaller guides were made so that they fitted together closely, and together were around the same size as the larger guide 3.
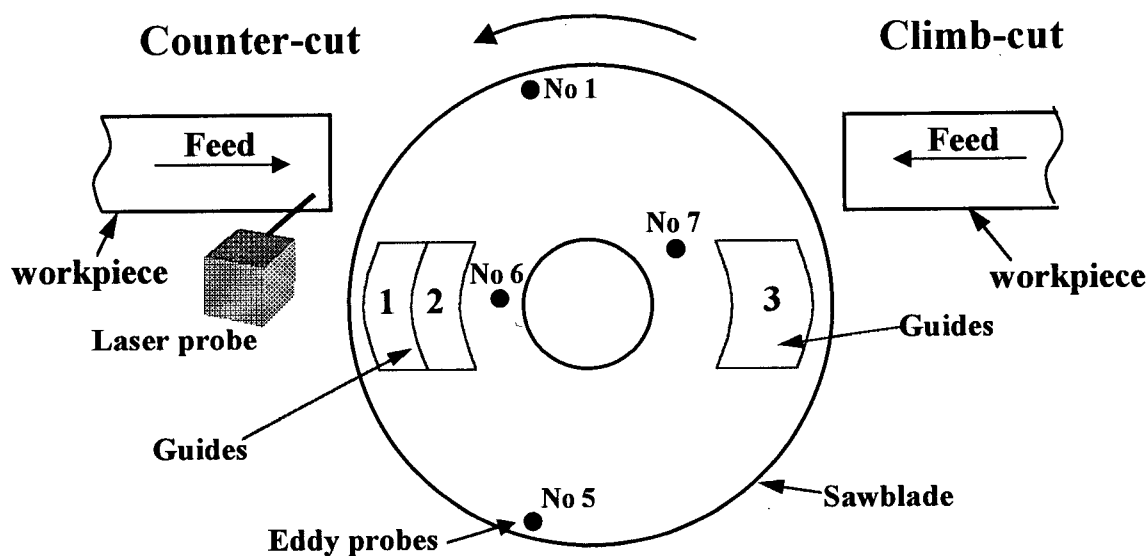
Figure 5.4: Schematic of the Various Guide Configurations and Different Feed Directions

The two saw-workpiece interaction mechanisms were examined as follows:

1. Saw Body - Workpiece Interaction: The "rudder" action of the saw described in Chapter 4 was investigated by changing the amount of guiding from minimal (guide 1 alone), to moderate (guides 1 and 2 together), and finally to massive (all guides 1, 2 and 3). In this sequence, the "rudder" action is reduced and the lateral stiffness of the saw is increased. If "rudder" action is the more important factor, the cutting accuracy will decrease. On the other hand, if lateral stiffness is the more important factor, the cutting accuracy will increase. For all these cutting tests, the workpiece feed direction was from the left to the right, corresponding to counter-cutting shown in figure 5.4.

2. Saw Tooth - Workpiece Interaction: For this interaction mechanism, the cutting tests were done by changing the workpiece feed direction to climb-cutting. Then the cutting accuracy for climb-cutting was compared with that of counter-cutting. The amount of guiding was varied from moderate (guide 3 alone), to massive (all guides 1, 2 and 3).

In this part of the experimental study, it was desired to cover as wide a range of saw operating conditions as possible. Again, the main parameters of interest were saw rotation speed and saw tensioning. Figure 5.5 shows a schematic diagram of the critical and dishing speeds of a circular saw as a function of the amount of tensioning. This diagram is similar to figure 3.9, but covers a wider range of rotation speeds and tensioning states. The inner rectangle indicates the range of figure 3.9. The eight saw operating conditions along the diagonal line in figure 5.5 was chosen for the present cutting tests.
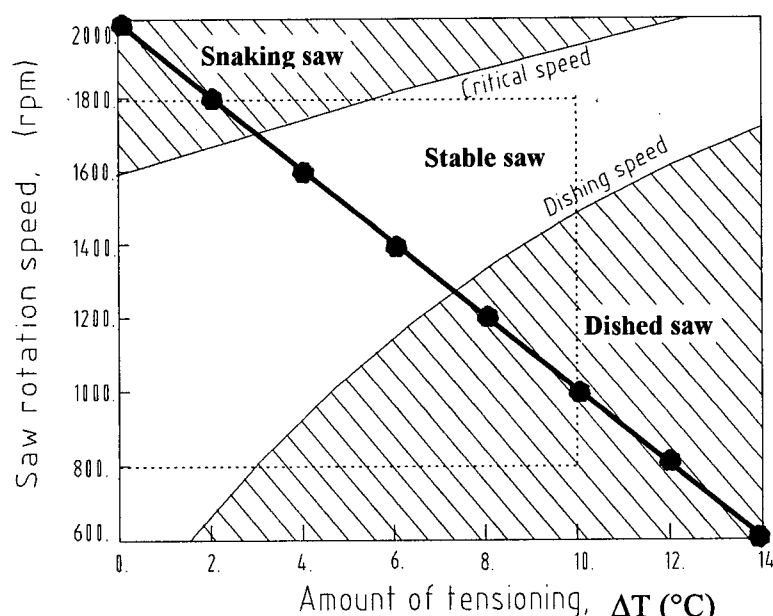
Figure 5.5: Relationship Between the Critical and Dishing Speeds of a Fixed-Collar Circular Saw and the Amount of Tensioning

Compilation of a diagram like figure 3.9 needs a very large number of measurements. Ideally, the most detailed information would be given by measuring every combination of rotation speed and thermal tensioning, as was done previously. However, this is an extremely time consuming task, one that is not a practical choice when there are as many as the five different sawing configurations to be considered here. Therefore, the present measurements were concentrated along the diagonal solid line shown in figure 5.5. This diagonal line was chosen because it spans the maximum range of saw operating conditions

from dishing to critical speed instability. Each of eight points in this diagonal line represents a sawing condition for a specified guide and sawing configuration.

During each cut, sawblade lateral displacement was detected at the four positions shown in figure 5.4. After removal of the sawn pieces, the two laser displacement probes measured the height profiles along the top and bottom edges of the sawn surface shown in figure 5.1.

In the cutting tests, for each of eight sawing conditions along the diagonal solid line shown in figure 5.5, four or six cuts were made to provide a statistically significant amount of experimental data. These sawing conditions covered the range from 2000 rpm and thermal tensioning $\Delta T = 0°C$ to 600 rpm and $\Delta T = 14°C$, in intervals of 200 rpm and $\Delta T = 2°C$. In the cutting tests, the gullet feed index was maintained at 0.30 and the corresponding feed per tooth was 0.047" by adjusting the workpiece feed speed for each sawing condition. The feed speeds of the guided saws are shown in Appendix.

The possible effects of tooth and guide wear can seriously complicate comparisons of saw performance. To minimize these complications, the sequence of cutting tests was selected so that these effects would be spread as equally as possible among the five different guide configurations. Sets of a cut at each of the eight sawing conditions along the diagonal solid line in figure 5.5 were achieved for each of the five guide configurations. The arrangement of the cutting test sequence for one cycle was shown in figure 5.6. This cycle was repeated so that at the end, six cuts had been made for most of the 40 combinations of sawing conditions and guide configurations. Because of operational difficulties, only four cuts could be achieved in each climb-cutting test.

The wood boards used in the cutting tests were selected to be as uniform as possible. In the experiments, all the tested boards were weighted and grouped into stacks of three that had almost the same total weight of around 60 kg. This practice has been found to

improve cutting uniformity [26]. Cutting tests with the same sawing condition, guide configuration and cutting direction were conducted in the different wood boards. This experimental arrangement helped randomize the variations in cutting performance due to natural differences in the wood boards and wear of the teeth. In total, 208 cuts were made using 54 wood boards.

Guide configurations & cutting directions	Eight sawing conditions							
	600 rpm 14 °C	800 rpm 12 °C	1000 rpm 10 °C	1200 rpm 8 °C	1400 rpm 6 °C	1600 rpm 4 °C	1800 rpm 2 °C	2000 rpm 0 °C
Guide 1 only (counter-cutting)								
Guide 1+2 (counter-cutting)								
Guide 1+2+3 (counter-cutting)								
Guide 1+2+3 (climb-cutting)								
Guide 3 only (climb-cutting)								
Guide 3 only (climb-cutting)								
Guide 1+2+3 (climb-cutting)								
Guide 1+2+3 (counter-cutting)								
Guide 1+2 (counter-cutting)								
Guide 1 only (counter-cutting)								

Arrows represent the directions of cutting test sequence.

Figure 5.6: Cutting Plan for One Cycle

2. Cutting Test Results

Figure 5.7 summarizes the results of the counter-cutting sawing tests. The lower three curves of this diagram show the standard deviations of the measured workpiece surface profiles cut by the guided saws in the three counter-cutting configurations and eight sawing conditions. Each point in the lower three curves is average of six measurements. The uppermost curve represents the standard deviations of the sawn surface profiles cut by a fixed-collar saw. These results correspond to a diagonal cross-section of figure 3.9.

In figure 5.7, the two vertical dashed lines represent the estimated critical and dishing speeds for the lower three curves. These two lines were obtained from the two intersection points of the diagonal solid line shown in figure 5.5 and the critical and dishing speed lines shown in figure 5.3. However, these two vertical lines do not apply to the uppermost curve with the fixed-collar configuration. The critical and dishing speed lines of the fixed-collar saw move to the left because the fixed-collar stiffens the saw and increases both the critical and dishing speeds. They are not shown in figure 5.7.
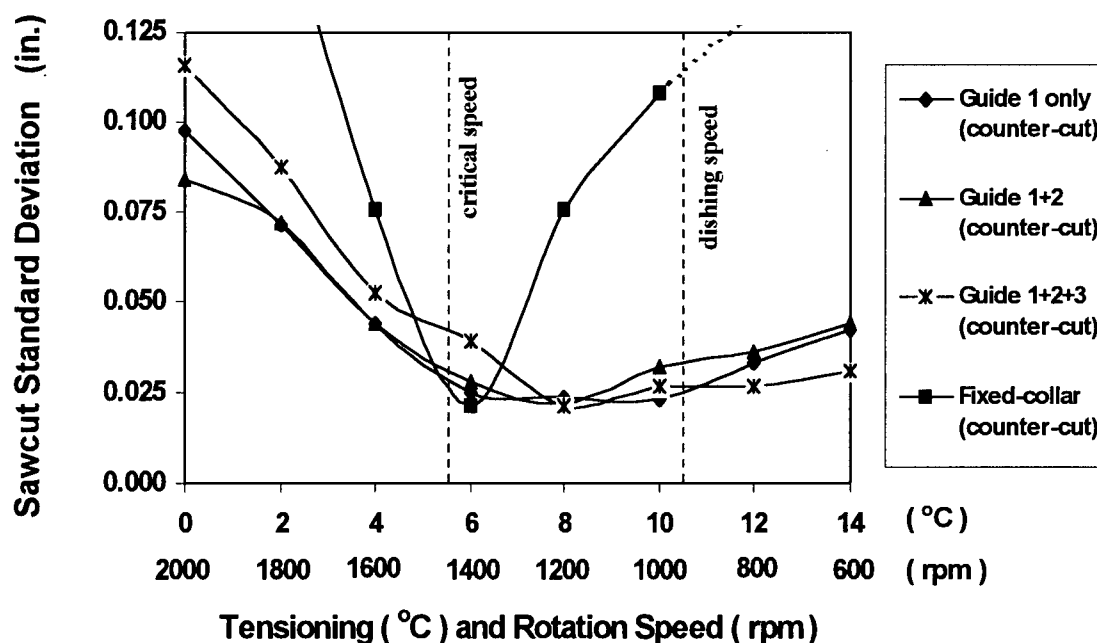
Figure 5.7: Measured Sawcut Standard Deviations of Counter-cutting Saws

In figure 5.7, the cutting behavior of three counter-cutting guided saws generally conforms to the expectations from the critical speed theory. On the left of the critical speed line, with the saw rotation speed increasing, the standard deviations increase quickly and the cutting accuracy deteriorates. This corresponds to the snaking saw area in figure 2.3, where unstable wavy sawcuts occur. On the right of the dishing speed line, where the saw becomes dished, the standard deviations also increase, although by a lesser amount. As expected from figure 5.5, the most stable operating condition can be achieved in the area between critical and dishing lines where minimum standard deviations can be obtained for all three guided saw configurations.

The most important point of figure 5.7 is the substantial reduction in the sawing standard deviations of the three guided counter-cutting saws when compared with a fixed-collar saw. On the left side of the diagram, the guides limit critical speed instability so that the standard deviations of the guided saws are greatly reduced. On the right side of the diagram, the guides help align the cutting edge of the dished saw, and only the downstream part of the dished saw inclines to one side. The "rudder" mechanism shown in figures 4.3 and 4.4 limits the sideways motion of the downstream part of the saw. On the other hand, in the case of the fixed-collar saw, the fixed-collar aligns the center area of the saw instead of the cutting edge. Therefore, when the saw dishes, the cutting edge of the saw moves to one side and the "rudder" mechanism in figures 4.1 and 4.2 then further helps this movement, causing the large sawcut standard deviation shown in the uppermost curve of figure 5.7.

The minimum standard deviations of the three guided saws are almost the same as that of the fixed-collar saw. However, the three guided saws are more tolerant of non-optimal conditions so that they can be operated within a larger operating range with acceptable cutting accuracy. In reality, this greater tolerance is not the only advantage of these guided saws. They also have the much greater cutting capacity that was observed in the preliminary experimental study. In figure 5.7, the gullet feed index of the guided saw data is 0.3. With the same sawblade mounted in a fixed-collar, the gullet feed index had to be

reduced to 0.09 to achieve acceptable cutting conditions. This gullet feed index of the fixed-collar saw corresponds to one third of the guided saw cutting rate. These results support that the "rudder" action as an important mechanism to describe the interaction between the saw body and workpiece. In figure 5.7, it is clear that the fixed-collar saw has the higher critical speed. Therefore, if critical speed were the only important factor, a greater cutting capacity would be expected for the fixed-collar saw.

Among the three standard deviation curves of the counter-cutting guided saws, on the left side of the diagram, the largest standard deviations (worst cutting accuracy) are obtained for three guides mounted on both sides of the sawblade. Again this result supports that the "rudder" action is an important mechanism to explain the interaction between saw body and workpiece. Therefore, if saw stiffness were the only important factor, this fully guided saw possessing the highest stiffness would cut wood more accurately.

From experimental observations, when operating in the critical speed region, the guided sawblade laterally moved from side to side in the sawcut and appeared to be very flexible. For the three counter-cutting guided configurations shown in figure 5.4, guide 3 limited the flexible movement and weakened the "rudder" action shown in figures 4.3 and 4.4.

On the right side of the dishing speed line, the standard deviations of the fully guided saw are slightly smaller than with the other two guided configurations. Saw dishing is produced by compressive radial stresses. The "rudder" action needed to push the dished shape of the sawblade back. Guide 3 helps align the back part of the sawblade for the three counter-cutting guide configuration shown in figure 5.4.

For the two counter-cutting cases of guides 1 and 1+2, from the experimental curves shown in figure 5.7, the size of the guide seems not to have much influence on cutting accuracy. In reality, the guides of both guide configurations are smaller than those typically used in sawmills. From the point of view of the "rudder" action, guided saws with these smaller guides were more flexible and consequently could be effective in

practice. The possible reason for not using smaller size guides is that the smaller guides have a higher wear rate. Figure 5.8 shows an example of guide wear. The favorable smaller guides should work properly and have a wear rate within permissible tolerance for a reasonable working life. In the present experiments, use of a larger guide was unpractical because it would influence the thermal tensioning system. The guide size was reduced only in the radial direction. A guide size reduction in the circumferential direction was not made because it would reduce stiffness without any significant influence on the "rudder" action.
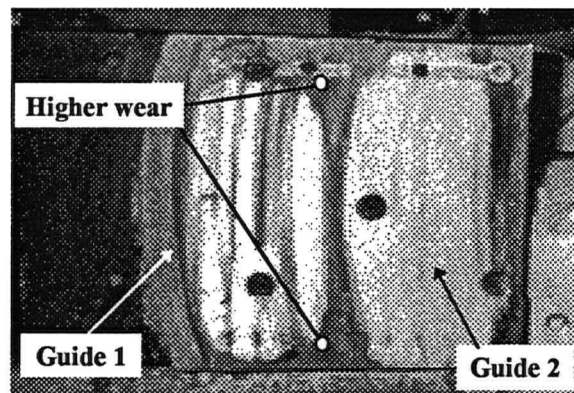
Figure 5.8: Guide Wear

Figure 5.9 shows the standard deviation curves for all five counter-cutting guided configurations and climb-cutting guided configurations. The counter-cutting curves are the same as the corresponding ones in figure 5.7. From figure 5.9, it is clear that the cutting standard deviations for climb-cutting was are generally much lower than for counter-cutting and almost independent of sawing conditions. Saw critical speed instability and saw dishing while climb-cutting do not have obvious influence on their sawcut standard deviations. These experimental results support that the interaction between saw tooth and workpiece shown in figure 4.5 is an important factor controlling saw cutting behavior.
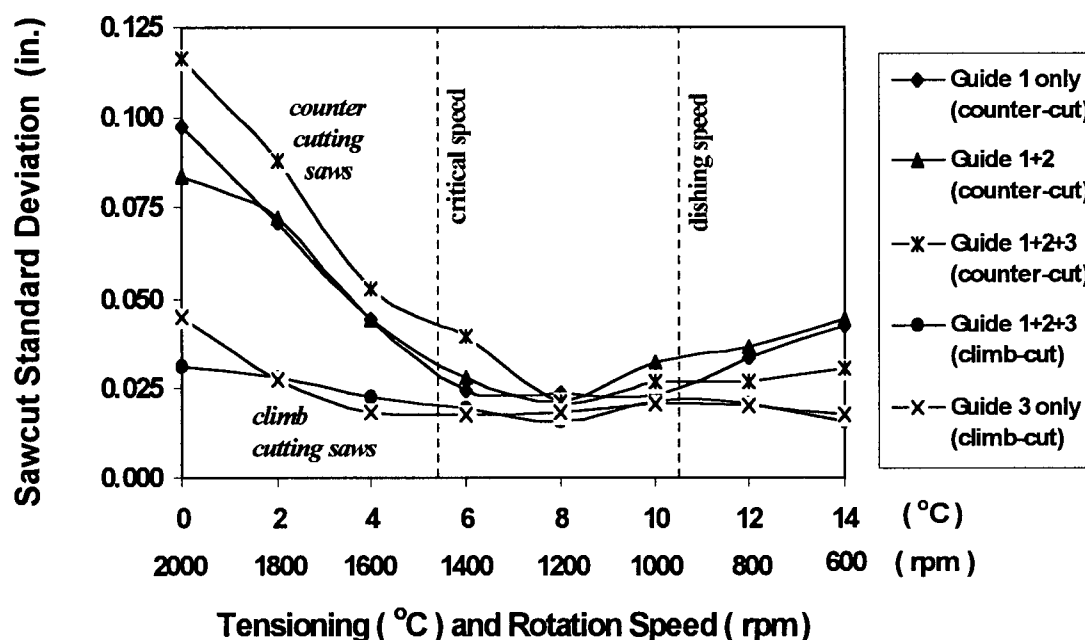
Figure 5.9: Measured Sawcut Standard Deviations of Guided Saws

Figures 5.10 and 5.11 provide some further insight into counter- and climb-cutting saw behavior. The right side of each figure shows the measured workpiece surface profiles (surface height vs. length) for a set of cuts made with a counter- and a climb-cutting guided saw at each of the eight operating conditions. The left side shows the corresponding sawblade vibration (lateral displacement vs. time) measured during the cuts. To assist interpretation, the time axes of these latter curves have been scaled horizontally so that they visually correspond to the workpiece surface profiles on the right. The tic marks on the horizontal axes indicate the period within which the saw was cutting. The cutting times range from about 2 seconds at 2000rpm, to about 6 seconds at 600rpm.

Saw Vibration   Workpiece Surface Profile
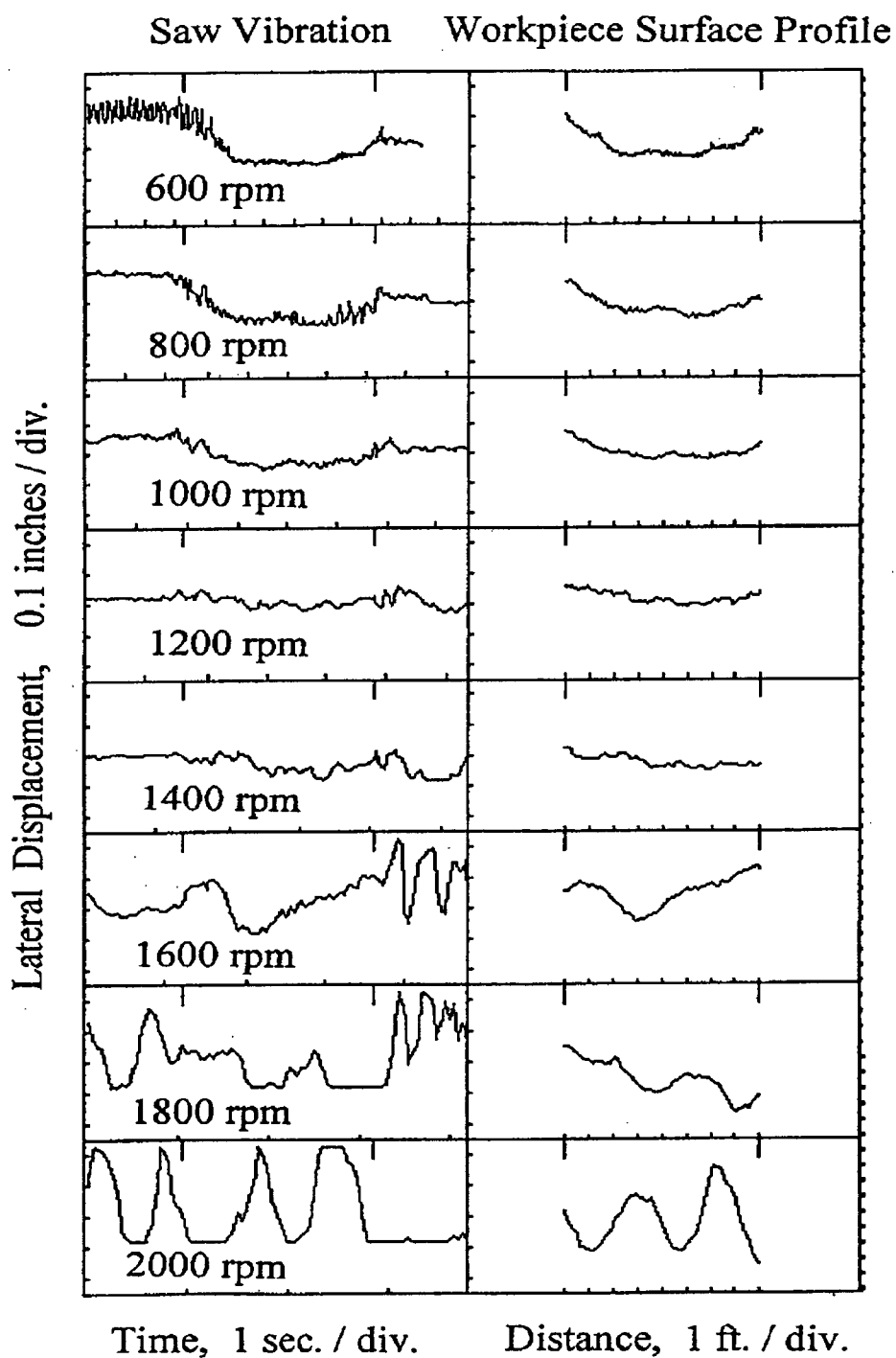
Figure 5.10: Saw vibration (left column) and workpiece surface profile (right column) measured with a counter-cutting saw with moderate guiding (guides 1 and 2). The vertical displacement scale is ±0.25" (±6.35 mm) within each graph box.
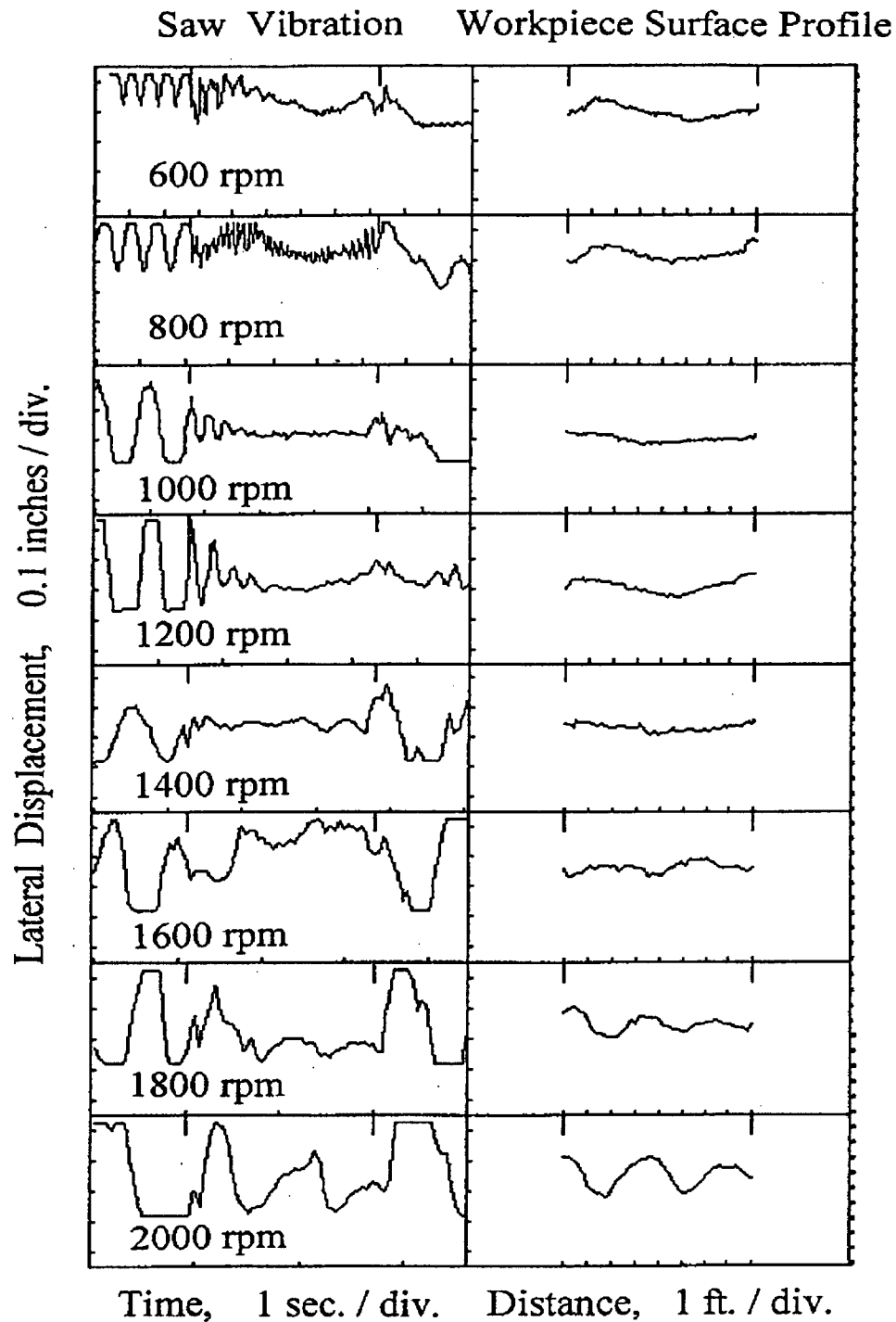
Figure 5.11: Saw vibration (left column) and workpiece surface profile (right column) measured with a climb-cutting saw with moderate guiding (guide 3). The vertical displacement scale is ±0.25" (±6.35 mm) within each graph box.

The saw behavior observed in figures 5.10 and 5.11 mirrors the standard deviation data in figure 5.9. In almost every case, the sawn surface profile closely follows the measured saw vibration during the corresponding interval. For the counter-cutting saw in figure 5.10, the saw vibration is the most stable and the sawcut profile straightest for sawing conditions in the middle range, at speed = 1200 rpm. At higher speeds, critical speed instability becomes increasingly apparent with the appearance of large low-frequency oscillations (snaking). The flat sections in the saw vibration curves indicate the limits of the measurement range of the displacement transducer that was used. The actual displacements in these regions were larger than indicated. The effects of saw dishing can be seen at the lowest speeds by the initial offsets in the saw displacements and sawn surface heights. Some self-centering occurs and these offsets reduce during cutting.

Broadly similar behavior can be seen for the climb-cutting saw in Figure 5.11. A notable distinguishing feature is the low frequency saw oscillation that occurs at all sawing conditions during idling before the sawcut. In all cases, this oscillation decays or entirely disappears during cutting. Only at supercritical speeds does some oscillation persist during the sawcut. Such unstable saw idling combined with stable wood cutting is a common observation in sawmills [25]. This large change in sawblade behavior between idling and cutting conditions is a dramatic demonstration of the effect of sawblade interaction with the workpiece. The right column of figure 5.11 confirms that the sawn surface profile produced by the climb-cutting saw is generally straighter than the corresponding profiles from the counter-cutting saw in figure 5.10.

5.3 Discussion

The purpose of this experimental study is to investigate saw-workpiece interactions by experimental observations and accordingly to give experimental support to the hypothesis that the interaction of the workpiece with the saw is the key factor controlling guided saw cutting behavior. The experimental results described above strongly show significant saw-workpiece interaction effects. The climb-cutting saw vibration curves shown in figure 5.11 exhibited the most dramatic example of these interaction results. The climb-cutting

sawblade oscillates greatly from side to side during idling, but this phenomenon immediately decays or disappears during cutting so that saw cutting becomes stable. On the other hand, the counter-cutting saw vibration curves shown in figure 5.10 generally become less stable during sawing. Both behaviors are believed to be closely connected to the stabilizing/destabilizing effects of tensile/compressive radial stresses in the sawblade, as shown in figure 4.5. Although the action of the radial stresses has an influence on sawing stability, at present it is still in its hypothetical stage. In the present tests, the action of the radial stresses can not provide an explanation why the large oscillations occur during idling of a climb-cutting saw. Of course, this can not be separated from the present measurements.

Saw body-workpiece interaction corresponding to the "rudder" action shown in figures 4.1 - 4.4 was clearly examined to be a key factor controlling saw cutting behavior. The unstable cutting behavior shown in figure 4.1 was clearly observed in a light cut with a fixed-collar saw during the preliminary experimental study. In that test, at a workpiece feed speed much lower than the speeds at which a similar guided saw is stable, the tested fixed-collar saw seriously inclined to one side, overheated and became permanently bent.

The "rudder" type shown in figure 4.3 and 4.4 was clearly determined to be a strong saw body-workpiece interaction mechanism by changing the guided configuration in the present experiments shown in figure 5.4. It was found that massive guiding using guides on both sides of a sawblade was detrimental to improving cutting accuracy. This coincides with industrial experience. It is because the additional guide on the outfeed side limits the "rudder" action of the saw. Contrary to expectations based on saw stiffness, a guided saw with quite small guides can cut wood accurately, as shown in figure 5.7. Observed from figure 5.7, the cutting accuracy using a small guide (guide 1 only) did not obviously differ from the one using a medium guide (guide 1+2). Both guides are smaller than those typically used in industry. This naturally introduces the question of whether or not it may be desirable to reduce the industrial guide size to increase the "rudder" action of guide saws. From the current experiments, a guided saw with a stiff cutting region

combined with a more flexible saw body may have an advantage in achieving better cutting accuracy. A small guide may be suitable for a curve sawing system so as to allow the flexible saw body to follow the curving sawcut more easily. On the other hand, in the experiments with the smallest guide (guide 1 only), a higher guide wear rate was observed, as shown in figure 5.8. This is probably the reason why sawmills don't commonly want to use smaller size guides. Perhaps, the observed guide wear problem is just the result of the extreme conditions in the experiments here. It is hoped that further study and industrial tests will be conducted to give insight into saw-workpiece interaction to answer the above questions.

The experimental results and observations do certainly give strong support to the hypothesis that the interactions between the saw and the workpiece are the key factors controlling guided saw cutting behavior and therefore a significant saw design factor. In Chapter 6, a theoretical model of a saw cutting a piece of wood will be developed to complement the present experimental results.

6.0 Theoretical Model

In this chapter, a simplified theoretical model of a saw cutting a workpiece is developed. The purpose of this model is to gain further insight into the interactions between the saw and workpiece.

To facilitate the gaining of a clear understanding of the basic phenomena involved, the theoretical model developed here has been made as simple as possible. Instead of modeling the sawblade as a circular plate, which would involve substantial mathematical complexity, the part of the saw interacting with the workpiece is instead modeled as a beam. Figure 6.1 shows the basis for this model. Figure 6.1(a) shows a circular saw cutting a workpiece.
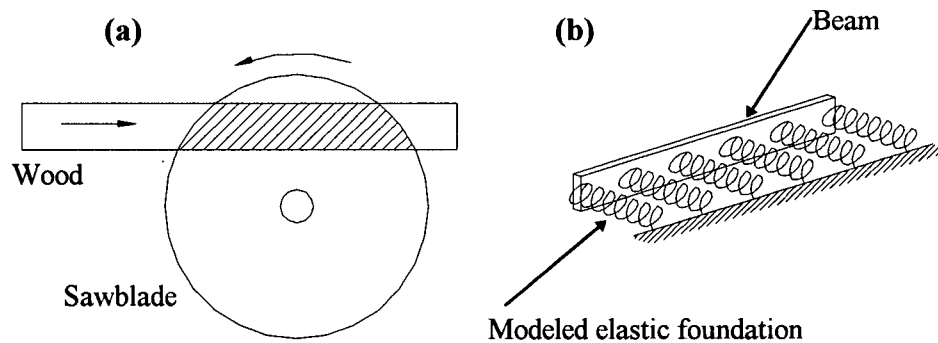
Figure 6.1: (a) A Circular Saw Cutting Wood, (b) Simplified Model of the Saw Using a Beam on an Elastic Foundation

The shaded area in Figure 6.1(a) indicates the overlap of the saw and the workpiece. This is the area for potential interactions. This area is modeled in Figure 6.1(b) by a rectangular beam of comparable dimensions to the shaded area in Figure 6.1(a). The beam is supported on an elastic foundation to simulate the effects of the guide and the remaining part of the sawblade. In general, this foundation has non-uniform stiffness. In the case of a guided saw, the foundation stiffness is greatest near the guides, while for a fixed-collar

saw, the foundation stiffness is greatest at the centre. In the following section, the beam model will be developed, starting from the simplest case.

6.1 Simple Beam with no External Constraints

A stationary sawblade without any constraints is modeled as a simple beam. The stiffness method [27] is used to analyze the simple beam bending.

1. Stiffness Matrix and Stiffness Equation of a Beam Element

A simple beam element is assumed to have a uniform cross section and a longitudinal axis along a single straight line (X axis). F_1 and F_2 are the forces vertically applied at nodes 1 and 2. u_1 and u_2 are the corresponding linear displacements. M_1 and M_2 are the moments applied at nodes 1 and 2. θ_1 and θ_2 are the corresponding angular displacements. The positive directions are shown in figure 6.2.
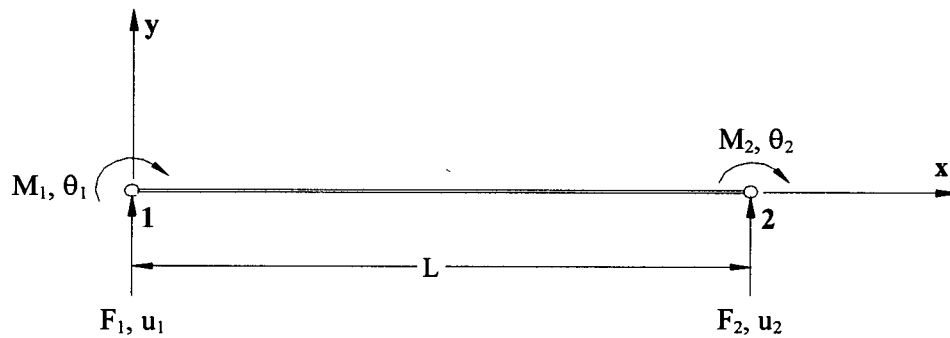
Figure 6.2: Nodal Forces and Displacements of a Beam Element

This beam element is also assumed to have a flexural rigidity EI over its length L and to be analyzed in the linear elastic range. The stiffness matrix of this basic beam element can be derived in the following way.

1. Case 1: $u_2 = \theta_2 = 0$

Under these boundary conditions, the beam element becomes a cantilever beam with support at node 2. From elementary beam theory [28, 29], displacements u_1 and θ_1 are:

$$u_1 = \frac{F_1 L^3}{3EI} + \frac{M_1 L^2}{2EI}$$
$$\theta_1 = \frac{F_1 L^2}{2EI} + \frac{M_1 L}{EI}$$

(6.1)

The above equations can be expressed in matrix form:

$$\frac{1}{EI}\begin{bmatrix} \dfrac{L^3}{3} & \dfrac{L^2}{2} \\ -\dfrac{6}{L^2} & L \end{bmatrix}\begin{Bmatrix} F_1 \\ M_1 \end{Bmatrix} = \begin{Bmatrix} u_1 \\ \theta_1 \end{Bmatrix}$$

(6.2)

which on inversion becomes:

$$EI\begin{bmatrix} \dfrac{12}{L^3} & -\dfrac{6}{L^2} \\ -\dfrac{6}{L^2} & \dfrac{4}{L} \end{bmatrix}\begin{Bmatrix} u_1 \\ \theta_1 \end{Bmatrix} = \begin{Bmatrix} F_1 \\ M_1 \end{Bmatrix}$$

(6.3)

Force and moment equilibrium gives following equations:

$$F_1 + F_2 = 0$$
$$F_1 L + M_1 + M_2 = 0$$

(6.4)

Substituting Eq. (6.4) into Eq. (6.1) and inverting gives

$$EI\begin{bmatrix} -\dfrac{12}{L^3} & \dfrac{6}{L^2} \\ -\dfrac{6}{L^2} & \dfrac{2}{L} \end{bmatrix}\begin{Bmatrix} u_1 \\ \theta_1 \end{Bmatrix} = \begin{Bmatrix} F_2 \\ M_2 \end{Bmatrix}$$

(6.5)

2. Case 2: $u_1 = \theta_1 = 0$

Under these boundary conditions, the beam element becomes a cantilever beam with support at node 1. Following the same procedure as before, the relationships between the forces and displacements are:

$$EI \begin{bmatrix} \dfrac{12}{L^3} & \dfrac{6}{L^2} \\ \dfrac{6}{L^2} & \dfrac{4}{L} \end{bmatrix} \begin{Bmatrix} u_2 \\ \theta_2 \end{Bmatrix} = \begin{Bmatrix} F_2 \\ M_2 \end{Bmatrix} \qquad (6.6)$$

and

$$EI \begin{bmatrix} -\dfrac{12}{L^3} & -\dfrac{6}{L^2} \\ \dfrac{6}{L^2} & \dfrac{2}{L} \end{bmatrix} \begin{Bmatrix} u_2 \\ \theta_2 \end{Bmatrix} = \begin{Bmatrix} F_1 \\ M_1 \end{Bmatrix} \qquad (6.7)$$

The general case can be obtained by superimposing the two possible distinct displacement states. This corresponds to $u_1 \neq 0$, $u_2 \neq 0$, $\theta_1 \neq 0$, $\theta_2 \neq 0$. Summing the results given in Eqs. (6.3), (6.5), (6.6), (6.7) gives Equation (6.8) which represents the stiffness equation for the general case.

$$K \begin{Bmatrix} u_1 \\ \theta_1 \\ u_2 \\ \theta_2 \end{Bmatrix} = \begin{Bmatrix} F_1 \\ M_1 \\ F_2 \\ M_2 \end{Bmatrix} \qquad (6.8)$$

$$K = EI \begin{bmatrix} \dfrac{12}{L^3} & -\dfrac{6}{L^2} & -\dfrac{12}{L^3} & -\dfrac{6}{L^2} \\ -\dfrac{6}{L^2} & \dfrac{4}{L} & \dfrac{6}{L^2} & \dfrac{2}{L} \\ -\dfrac{12}{L^3} & \dfrac{6}{L^2} & \dfrac{12}{L^3} & \dfrac{6}{L^2} \\ -\dfrac{6}{L^2} & \dfrac{2}{L} & \dfrac{6}{L^2} & \dfrac{4}{L} \end{bmatrix} \qquad (6.9)$$

Eq. (6.9) is the stiffness matrix for the basic beam element shown in figure 6.2. The calculation of the computer program is based on the stiffness equation and stiffness matrix.

2. Stiffness Matrix of a Beam Assemblage

Multiple elements are needed for the general case of a non-uniform beam with intermediate loads. At first, the beam assemblage considered here consists of two uniform beam elements as shown in figure 6.3. Each element has a given value for a flexural rigidity EI over its length L and is assumed to remain within the linear elastic range.
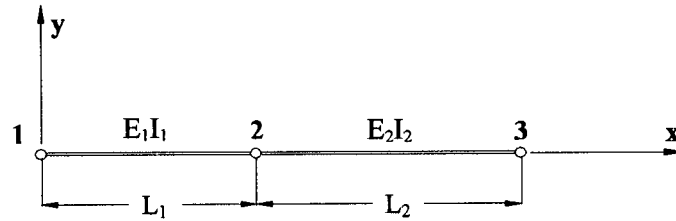
Figure 6.3: Beam Assemblage Consisting of Two Beam Elements

The stiffness matrix for the beam assemblage in figure 6.3 is of order 6×6, corresponding to the six degrees of freedom (3 nodes each 2 degrees of freedom at each node). This stiffness matrix is formed by superimposing the individual element stiffness matrices of the type shown in Eq. (6.9). Eq. (6.10) shows the resulting overall stiffness matrix for the beam assemblage. The dashed lines indicate the stiffness matrices for the individual beam elements.

$$
\begin{array}{cccccc}
u_1 & \theta_1 & u_2 & \theta_2 & u_3 & \theta_3
\end{array}
$$

$$
K = \begin{bmatrix}
\dfrac{12E_1I_1}{L_1^3} & -\dfrac{6E_1I_1}{L_1^2} & -\dfrac{12E_1I_1}{L_1^3} & -\dfrac{6E_1I_1}{L_1^2} & 0 & 0 \\[2ex]
-\dfrac{6E_1I_1}{L_1^2} & \dfrac{4E_1I_1}{L_1} & \dfrac{6E_1I_1}{L_1^2} & \dfrac{2E_1I_1}{L_1} & 0 & 0 \\[2ex]
-\dfrac{12E_1I_1}{L_1^3} & \dfrac{6E_1I_1}{L_1^2} & \dfrac{12E_1I_1}{L_1^3}+\dfrac{12E_2I_2}{L_2^3} & \dfrac{6E_1I_1}{L_1^2}-\dfrac{6E_2I_2}{L_2^2} & -\dfrac{12E_2I_2}{L_2^3} & -\dfrac{6E_2I_2}{L_2^2} \\[2ex]
-\dfrac{6E_1I_1}{L_1^2} & \dfrac{2E_1I_1}{L_1} & \dfrac{6E_1I_1}{L_1^2}-\dfrac{6E_2I_2}{L_2^2} & \dfrac{4E_1I_1}{L_1}+\dfrac{4E_2I_2}{L_2} & \dfrac{6E_2I_2}{L_2^2} & \dfrac{2E_2I_2}{L_2} \\[2ex]
0 & 0 & -\dfrac{12E_2I_2}{L_2^3} & \dfrac{6E_2I_2}{L_2^2} & \dfrac{12E_2I_2}{L_2^3} & \dfrac{6E_2I_2}{L_2^2} \\[2ex]
0 & 0 & -\dfrac{6E_2I_2}{L_2^2} & \dfrac{2E_2I_2}{L_2} & \dfrac{6E_2I_2}{L_2^2} & \dfrac{4E_2I_2}{L_2}
\end{bmatrix}
$$

$$\ldots\ldots\ldots\ldots (6.10)$$

For any other multiple elements in a simple beam, the gross stiffness matrices can be obtained by superimposing additional beam element stiffness matrices. The gross stiffness matrices are block tridiagonal and can be conveniently solved using a standard solver [34].

6.2 A Simple Beam on Elastic Foundation

The simple beam model in figure 6.1 (b) includes an elastic foundation. This foundation represents the support provided to the beam by the unshaded part of the sawblade shown in figure 6.1 (a) and any guides. The foundation stiffness is modeled as linear springs at the nodes, as shown in figure 6.4.
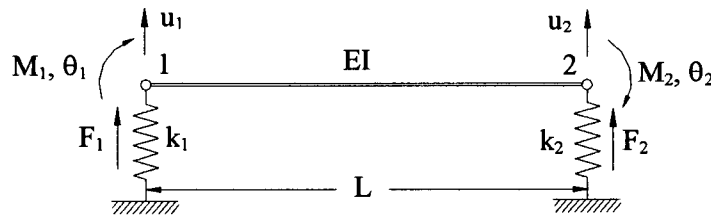
Figure 6.4: One Element Beam on the Elastic Foundation Modeled as Two Nodal Linear Springs

The stiffnesses of the two linear springs are

$$k_1 = k_2 = \frac{k_f L}{2} \tag{6.11}$$

where k_f is the foundation stiffness per unit length.

The two foundation springs augment the stiffness matrix shown in Eq. (6.9) to

$$K = EI \begin{bmatrix} \dfrac{12}{L^3} + \dfrac{k_1}{EI} & & \text{SYM.} & \\ -\dfrac{6}{L^2} & \dfrac{4}{L} & & \\ -\dfrac{12}{L^3} & \dfrac{6}{L^2} & \dfrac{12}{L^3} + \dfrac{k_2}{EI} & \\ -\dfrac{6}{L^2} & \dfrac{2}{L} & \dfrac{6}{L^2} & \dfrac{4}{L} \end{bmatrix} \tag{6.12}$$

For the multi-element beam, the gross stiffness matrix can be obtained by the beam assemblage method shown in Section 6.1.

The augmented matrix was incorporated into the computer program. This program was tested by comparing its calculated results with an analytical solution. For the "long" beam on an elastic foundation shown in figure 6.4, the analytical solution [30] is:

Displacements
$$y = \frac{F\beta}{2k_f} e^{-\beta x} \left(\cos\beta x + \sin\beta x \right)$$
(6.13)

where
$$\beta = \sqrt[4]{\frac{k_f}{4EI}}$$
(6.14)

and for a "long" beam $\beta L > 5$.

When using 5 equal beam elements, the numerical solution was within 9% of the analytical result. For ten elements, the maximum difference was 1.2%, and for 20 elements the maximum difference was 0.2%.

6.3 Several Added Factors

The following several features were also added to the computer program.

1. Transverse Springs at Ends of Beam

Stiffnesses due to transverse springs were added to the ends of the beam assemblage to provide a means of external support. This addition allowed test calculations to be done with simply supported beam configurations. Comparison of the results of these calculations with analytical solutions confirmed the correct functioning of the beam calculation.

2. Rotational Springs at Ends of Beam

Stiffnesses due to rotational springs were also added to the ends of the beam assemblage to provide further means of external support. This addition allowed further test calculations to be done with "built-in" external supports. Again, comparison of the results

of these calculations with analytical solutions confirmed the correct functioning of the beam calculation.

3. Non-Uniform Flexural Rigidity EI

In general, the flexural rigidity EI of a beam can vary along its length. The stiffness matrix of the computer program includes this factor. For the case of the flexural rigidity changing linearly along the beam, when using 5, 10 and 25 equal beam elements, the numerical solutions were within 3.7%, 1.8% and 0.42% of the analytical results respectively.

4. Foundation Displacements
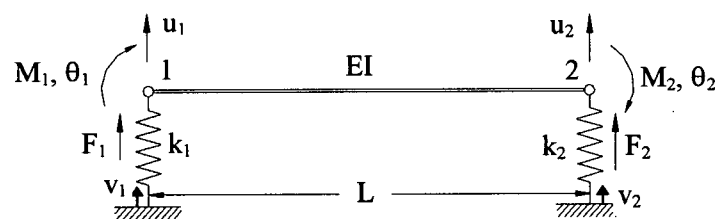
Figure 6.5: Adding Foundation Displacements to One Element Beam on the Elastic Foundation at Two Nodes

Figure 6.5 shows that nodes 1 and 2 are given foundation displacement v_1 and v_2. For node 1, the original nodal displacement relative to the fixed space is u_1. Therefore,

$$\text{Spring extension} = u_1 - v_1 \tag{6.15}$$

$$\text{Spring force} = -k_1(u_1 - v_1) \tag{6.16}$$

For node 2, the spring extension and spring force can be obtained in the same way as in Equations (6.15) and (6.16).

The stiffness equation can be obtained by using the gross stiffness matrix K shown in Eq. (6.12). Therefore, by adding foundation displacements, the stiffness equation for the case shown in figure 6.5 becomes

$$K \begin{Bmatrix} u_1 \\ \theta_1 \\ u_2 \\ \theta_2 \end{Bmatrix} = \begin{Bmatrix} F_1 + k_1 v_1 \\ M_1 \\ F_2 + k_2 v_2 \\ M_2 \end{Bmatrix} \qquad (6.17)$$

where v_1 and v_2 are the added foundation displacements, and K is the same as Eq. (6.12). These added foundation displacements were included in the computer program in preparation for later sawblade-workpiece interaction calculations.

6.4 Beam with Axial Force

In wood cutting, the compressive radial force created by cutting the workpiece is a possible factor producing unstable cutting behavior. This factor can be included in the theoretical calculation of the beam model as an axial force in the beam.

Figure 6.6 shows a one-element beam subjected to various forces and moments at its nodes. It is assumed that the axial force does not significantly change the beam moments, the axial displacement is negligible, all the forces act in one plane and that all deflections are linearly elastic. F_1 and F_2 are the forces vertically applied at nodes 1 and 2. u_1 and u_2 are the corresponding linear displacements. M_1 and M_2 are the moments applied at nodes 1 and 2. θ_1 and θ_2 are the corresponding angular displacements. H is the axial force applied at nodes 1 and 2. The positive directions are shown in figure 6.6. The stiffness matrix of this basic beam element can be derived in the following way.
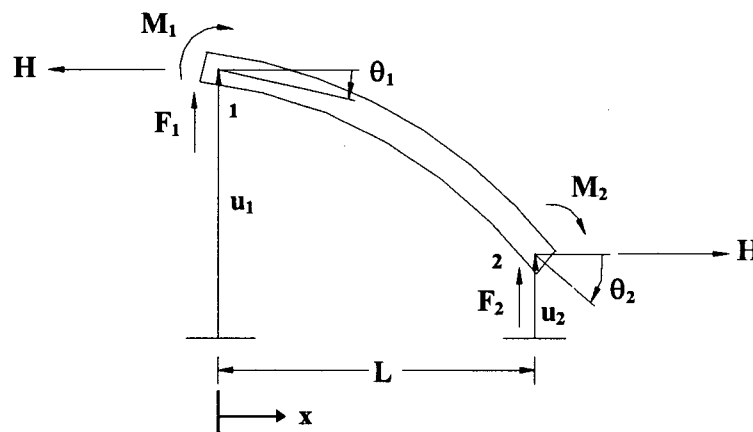
Figure 6.6: Forces and Displacements at Two Nodes of One Element Beam

1. Case 1: $u_1 \neq 0$, $u_2 = \theta_1 = \theta_2 = 0$, *as shown in figure 6.7.*
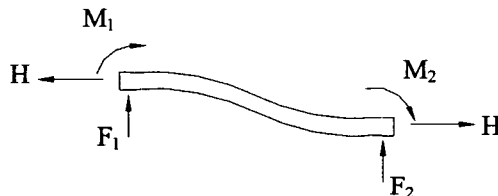
Figure 6.7: Beam Deformation Subjected to Nodal Forces
($u_1 \neq 0$, $u_2 = \theta_1 = \theta_2 = 0$)

From beam theory [29, 31] and equilibrium condition, the applied forces in terms of displacement u_1 and axial force H are

$$F_1 = \left(\frac{12EI}{L^3} + \frac{H}{L} \right) u_1 \qquad (6.18)$$

$$M_1 = -\frac{6EI}{L^2} u_1 \qquad (6.19)$$

$$F_2 = -\left(\frac{12EI}{L^3} + \frac{H}{L} \right) u_1 \qquad (6.20)$$

$$M_2 = -\frac{6EI}{L^2} u_1 \qquad (6.21)$$

2. Case 2: $\theta_1 \neq 0$, $u_1 = u_2 = \theta_2 = 0$, *as shown in figure 6.8.*
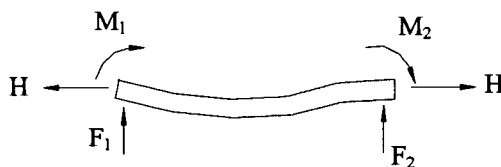
Figure 6.8: Beam Deformation Subjected to Nodal Forces
($\theta_1 \neq 0$, $u_1 = u_2 = \theta_2 = 0$)

From beam theory [29, 31] and equilibrium condition, the applied forces in terms of displacement θ_1 are

$$F_1 = -\frac{6EI}{L^2}\theta_1 \tag{6.22}$$

$$M_1 = \frac{4EI}{L}\theta_1 \tag{6.23}$$

$$F_2 = \frac{6EI}{L^2}\theta_1 \tag{6.24}$$

$$M_2 = \frac{2EI}{L}\theta_1 \tag{6.25}$$

3. *Case 3:* $u_2 \neq 0$, $u_1 = \theta_1 = \theta_2 = 0$, *as shown in figure 6.9.*
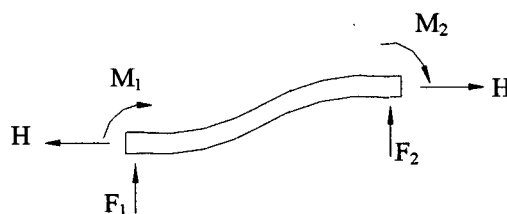
Figure 6.9: Beam Deformation Subjected to Nodal Forces
($u_2 \neq 0$, $u_1 = \theta_1 = \theta_2 = 0$)

From beam theory [29, 31] and equilibrium condition, the applied forces in terms of displacement u_2 and axial force H, similar to Equations (6.18) - (6.21), can be obtained.

4. *Case 4:* $\theta_2 \neq 0$, $u_1 = u_2 = \theta_1 = 0$, *as shown in figure 6.10.*
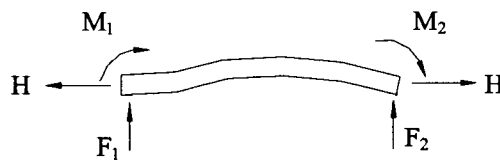
Figure 6.10: Beam Deformation Subjected to Nodal Forces
($\theta_2 \neq 0$, $u_1 = u_2 = \theta_1 = 0$)

From beam theory [29, 31] and equilibrium condition, the applied forces in terms of displacement θ_2, similar to Equations (6.22) - (6.25), can be obtained.

The general case can be obtained by summing the above four cases.

$$F_1 = \left(\frac{12EI}{L^3} + \frac{H}{L}\right)u_1 - \frac{6EI}{L^2}\theta_1 - \left(\frac{12EI}{L^3} + \frac{H}{L}\right)u_2 - \frac{6EI}{L^2}\theta_2 \qquad (6.26)$$

$$M_1 = -\frac{6EI}{L^2}u_1 + \frac{4EI}{L}\theta_1 + \frac{6EI}{L^2}u_2 + \frac{2EI}{L}\theta_2 \qquad (6.27)$$

$$F_2 = -\left(\frac{12EI}{L^3} + \frac{H}{L}\right)u_1 + \frac{6EI}{L^2}\theta_1 + \left(\frac{12EI}{L^3} + \frac{H}{L}\right)u_2 + \frac{6EI}{L^2}\theta_2 \qquad (6.28)$$

$$M_2 = -\frac{6EI}{L^2}u_1 + \frac{2EI}{L}\theta_1 + \frac{6EI}{L^2}u_2 + \frac{4EI}{L}\theta_2 \qquad (6.29)$$

When adding an elastic foundation (modeled as two linear springs k_1 and k_2) shown in figure 6.4, the stiffness matrix becomes

$$K = \begin{bmatrix} \left(\dfrac{12EI}{L^3} + \dfrac{H}{L} + k_1\right) & & & \text{SYM.} \\ -\dfrac{6EI}{L^2} & \dfrac{4EI}{L} & & \\ -\left(\dfrac{12EI}{L^3} + \dfrac{H}{L}\right) & \dfrac{6EI}{L^2} & \left(\dfrac{12EI}{L^3} + \dfrac{H}{L} + k_2\right) & \\ -\dfrac{6EI}{L^2} & \dfrac{2EI}{L} & \dfrac{6EI}{L^2} & \dfrac{4EI}{L} \end{bmatrix} \qquad (6.30)$$

It is clear that when axial force $H = 0$, the stiffness matrix shown in Eq. (6.30) is the same as that shown in Eq. (6.12).
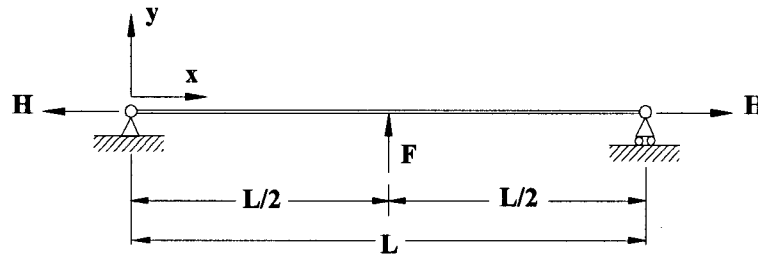
Figure 6.11: Beam with Combined Axial and Lateral Forces

Figure 6.11 shows a beam subjected to axial and lateral forces. In this case, the middle displacement is [30, 31]

$$y = -\frac{F}{2kP}\left(\tan\frac{kL}{2} - \frac{kL}{2}\right)$$ (6.31)

where P = -H and

$$k = \sqrt{\frac{P}{EI}}$$ (6.32)

P can be represented as

$$P = \frac{(kL)^2 EI}{L^2}$$ (6.33)

When kL = π, P is Euler buckling load P_{CR}

$$P = \frac{\pi^2 EI}{L^2}$$ (6.34)

The centre displacements of the beam calculated from the computer program using 30 elements were compared with the centre displacements from the above theoretical formulae.

The more elements used for these calculations, the better the accuracy of the numerical results. For kL = 3.0, when using 6, 10, 16, 20 and 30 equal beam elements, the numerical solutions were within 17.6%, 6.4%, 1.8%, 0.64%, and 0.53% of the analytical results respectively.

Equation (6.31) shows unbounded response (buckling) when kL = π = 3.1416. The numerical calculation using 30 equal elements showed a similar unbounded response at kL = 3.1430. The agreement between these results is very satisfactory.

6.5 Stiffness Matrix for a Moving Beam

When modeling a saw cutting a workpiece, saw rotation speed is an important factor that needs to be considered in the computer calculation. Figure 6.12 shows one beam element similar to that shown in figure 6.2, except that it is moving axially with a speed V.
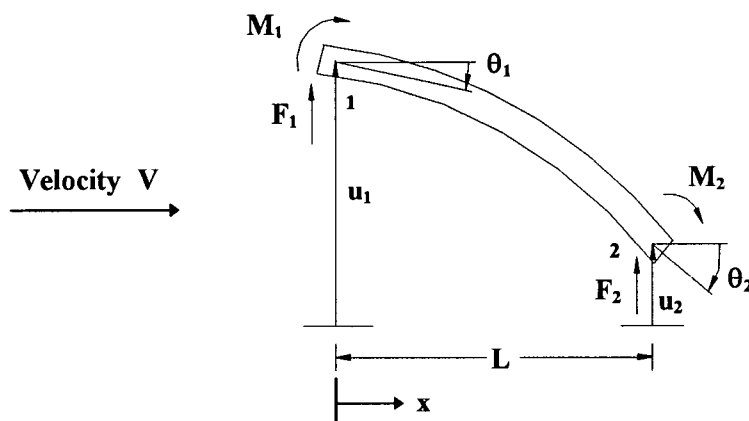
Figure 6.12: Forces and Displacements at Two Nodes of One Moving Element Beam

For vibration of the beam with loads only at the ends, the differential equation [32, 33] is

$$EI\frac{\partial^4 u}{\partial x^4} + m\frac{D^2 u}{Dt^2} = 0 \tag{6.35}$$

where m is mass per unit length and $\dfrac{D}{Dt}$ is the differential operator associated with the coordinate system attached to the moving beam. If $\dfrac{\partial}{\partial t}$ is the equivalent operator for the coordinate system fixed in space, then transformation relative to a fixed coordinate system [33] is

$$\frac{D}{Dt} = \frac{\partial}{\partial t} + V\frac{\partial}{\partial x} \tag{6.36}$$

where V is the beam velocity. After substituting Eq. (6.36) into Eq. (6.35), Eq. (6.35) becomes

$$\frac{EI}{m}\frac{\partial^4 u}{\partial x^4} + \frac{\partial^2 u}{\partial t^2} + 2V\frac{\partial^2 u}{\partial x \partial t} + V^2\frac{\partial^2 u}{\partial x^2} = 0 \qquad (6.37)$$

For constant loads and steady state conditions, all time derivatives are zero. $\frac{\partial}{\partial x}$ can be replaced by $\frac{d}{dx}$, and Eq. (6.37) becomes

$$\frac{EI}{m}\frac{d^4 u}{dx^4} + V^2\frac{d^2 u}{dx^2} = 0 \qquad (6.38)$$

The general solution for Eq. (6.38) is

$$u = A\cos\lambda x + B\sin\lambda x + Cx + D \qquad (6.39)$$

where

$$\lambda = \sqrt{\frac{mV^2}{EI}} \qquad (6.40)$$

1. Case 1: $u_1 \neq 0$, $u_2 = \theta_1 = \theta_2 = 0$, as shown in figure 6.7(no axial force H).

Solutions to the coefficients A, B, C and D in Eq. (6.39) are

$$A = \frac{1 - \cos\lambda L}{2 - 2\cos\lambda L - \lambda L\sin\lambda L}u_1 \qquad (6.41)$$

$$B = \frac{-\sin\lambda L}{2 - 2\cos\lambda L - \lambda L\sin\lambda L}u_1 \qquad (6.42)$$

$$C = \frac{\lambda\sin\lambda L}{2 - 2\cos\lambda L - \lambda L\sin\lambda L}u_1 \qquad (6.43)$$

$$D = \frac{1 - \cos\lambda L - \lambda L\sin\lambda L}{2 - 2\cos\lambda L - \lambda L\sin\lambda L}u_1 \qquad (6.44)$$

The applied forces in terms of displacement u_1 and λ are

$$F_1 = \frac{EI\lambda^3\sin\lambda L}{2 - 2\cos\lambda L - \lambda L\sin\lambda L}u_1 \qquad (6.45)$$

$$M_1 = \frac{-EI\lambda^2(1 - \cos\lambda L)}{2 - 2\cos\lambda L - \lambda L \sin\lambda L} u_1 \qquad (6.46)$$

$$F_2 = \frac{-EI\lambda^3 \sin\lambda L}{2 - 2\cos\lambda L - \lambda L \sin\lambda L} u_1 \qquad (6.47)$$

$$M_2 = \frac{-EI\lambda^2(1 - \cos\lambda L)}{2 - 2\cos\lambda L - \lambda L \sin\lambda L} u_1 \qquad (6.48)$$

2. *Case 2:* $\theta_1 \neq 0$, $u_1 = u_2 = \theta_2 = 0$, *as shown in figure 6.8 (no axial force H).*

The applied forces in terms of displacement θ_1 and λ are

$$F_1 = \frac{EI\lambda^2(1 - \cos\lambda L - \lambda L \sin\lambda L)}{2 - 2\cos\lambda L - \lambda L \sin\lambda L} \theta_1 \qquad (6.49)$$

$$M_1 = \frac{EI\lambda \ (\sin\lambda L - \lambda L \cos\lambda L)}{2 - 2\cos\lambda L - \lambda L \sin\lambda L} \theta_1 \qquad (6.50)$$

$$F_2 = \frac{EI\lambda^2(1 - \cos\lambda L)}{2 - 2\cos\lambda L - \lambda L \sin\lambda L} \theta_1 \qquad (6.51)$$

$$M_2 = \frac{EI\lambda \ (\lambda L - \sin\lambda L)}{2 - 2\cos\lambda L - \lambda L \sin\lambda L} \theta_1 \qquad (6.52)$$

3. *Case 3:* $u_2 \neq 0$, $u_1 = \theta_1 = \theta_2 = 0$, *as shown in figure 6.9 (no axial force H).*

The applied forces in terms of displacement u_2 and λ are

$$F_1 = \frac{-EI\lambda^3 \sin\lambda L}{2 - 2\cos\lambda L - \lambda L \sin\lambda L} u_2 \qquad (6.53)$$

$$M_1 = \frac{EI\lambda^2(1 - \cos\lambda L)}{2 - 2\cos\lambda L - \lambda L \sin\lambda L} u_2 \qquad (6.54)$$

$$F_2 = \frac{EI\lambda^3 \sin\lambda L}{2 - 2\cos\lambda L - \lambda L \sin\lambda L} u_2 \qquad (6.55)$$

$$M_2 = \frac{EI\lambda^2(1 - \cos\lambda L)}{2 - 2\cos\lambda L - \lambda L \sin\lambda L} u_2 \qquad (6.56)$$

4. Case 4: $\theta_2 \neq 0$, $u_1 = u_2 = \theta_1 = 0$, *as shown in figure 6.10 (no axial force H).*

The applied forces in terms of displacement θ_2 and λ are

$$F_1 = \frac{-EI\lambda^2(1-\cos\lambda L)}{2-2\cos\lambda L - \lambda L \sin\lambda L}\theta_2 \qquad (6.57)$$

$$M_1 = \frac{EI\lambda\ (\lambda L - \sin\lambda L)}{2-2\cos\lambda L - \lambda L \sin\lambda L}\theta_2 \qquad (6.58)$$

$$F_2 = \frac{-EI\lambda^2(1-\cos\lambda L - \lambda L \sin\lambda L)}{2-2\cos\lambda L - \lambda L \sin\lambda L}\theta_2 \qquad (6.59)$$

$$M_2 = \frac{EI\lambda\ (\sin\lambda L - \lambda L \cos\lambda L)}{2-2\cos\lambda L - \lambda L \sin\lambda L}\theta_2 \qquad (6.60)$$

The axial force H and the foundation spring k_1 and k_2 are not considered in the above four cases. These factors can be included in the above four cases using the same method as described in Sections 6.2 and 6.4. The resulting stiffness matrix is:

$$K = \begin{bmatrix} \left(\dfrac{\lambda^3 EI \sin\lambda L}{\Delta} + \dfrac{H}{L} + k_1\right) & \dfrac{\lambda^2 EI(1-\cos\lambda L - \lambda L \sin\lambda L)}{\Delta} & -\left(\dfrac{\lambda^3 EI \sin\lambda L}{\Delta} + \dfrac{H}{L}\right) & \dfrac{-\lambda^2 EI(1-\cos\lambda L)}{\Delta} \\[2ex] \dfrac{-\lambda^2 EI(1-\cos\lambda L)}{\Delta} & \dfrac{\lambda\ EI(\sin\lambda L - \lambda L \cos\lambda L)}{\Delta} & \dfrac{\lambda^2 EI(1-\cos\lambda L)}{\Delta} & \dfrac{\lambda\ EI(\lambda L - \sin\lambda L)}{\Delta} \\[2ex] -\left(\dfrac{\lambda^3 EI \sin\lambda L}{\Delta} + \dfrac{H}{L}\right) & \dfrac{\lambda^2 EI(1-\cos\lambda L)}{\Delta} & \left(\dfrac{\lambda^3 EI \sin\lambda L}{\Delta} + \dfrac{H}{L} + k_2\right) & \dfrac{\lambda^2 EI(1-\cos\lambda L - \lambda L \sin\lambda L)}{\Delta} \\[2ex] \dfrac{-\lambda^2 EI(1-\cos\lambda L)}{\Delta} & \dfrac{\lambda\ EI(\lambda L - \sin\lambda L)}{\Delta} & \dfrac{\lambda^2 EI(1-\cos\lambda L)}{\Delta} & \dfrac{\lambda\ EI(\sin\lambda L - \lambda L \cos\lambda L)}{\Delta} \end{bmatrix}$$

$$\ldots\ldots\ldots (6.61)$$

$$\Delta = 2 - 2\cos\lambda L - \lambda L \sin\lambda L \qquad (6.62)$$

K is the stiffness matrix of the basic moving beam element with additional horizontal axial force H. After the beam velocity is considered, the calculation of the computer program is based on the stiffness matrix shown in Eq. (6.61).

The denominator Δ is zero in Eq. (6.61) when $\lambda L = 0$, 2π, 8.987, 4π, 15.45, 6π etc. The first value, $\lambda L = 0$, corresponds to the case of a stationary beam element ($V = 0$). The second value, $\lambda L = 2\pi$, corresponds to the case of a beam element moving at its first critical speed. This critical speed is:

$$V_{1stCR} = \frac{2\pi}{L} \sqrt{\frac{EI}{m}} \qquad (6.63)$$

For a stationary beam, Eq. (6.61) is undefined, and Eq. (6.30) must be used instead. In the computer program, Eq. (6.30) was used when $V \leq 0.001 V_{1stCR}$ to avoid numerical round-off error when Δ is very small.

For all the cases mentioned before, such as adding springs at two ends and adding foundation displacements and so on, the calculations were conducted again using the stiffness matrices for moving beam and stationary beam. The results from these calculations were the same as the ones calculated before.

6.6 Sawcut Simulations

The numerical model previously described was used to create a simulation of the behavior of a saw during wood cutting. This was done by further modifying the computer program so that it simulated a workpiece passing along the beam model. The simulation was achieved by considering a series of small time increments and advancing the workpiece past the sawblade in corresponding steps.

Figure 6.13 shows a beam representing a saw, contained within a sawcut. The workpiece moves from left to right. Saw teeth are assumed to exist at the cutting edge. The side clearance of these teeth results in a kerf width greater than the beam width. Transverse cutting forces applied at the cutting edge can move the saw teeth sideways. The sawcut surfaces represent the history of this sideways motion.
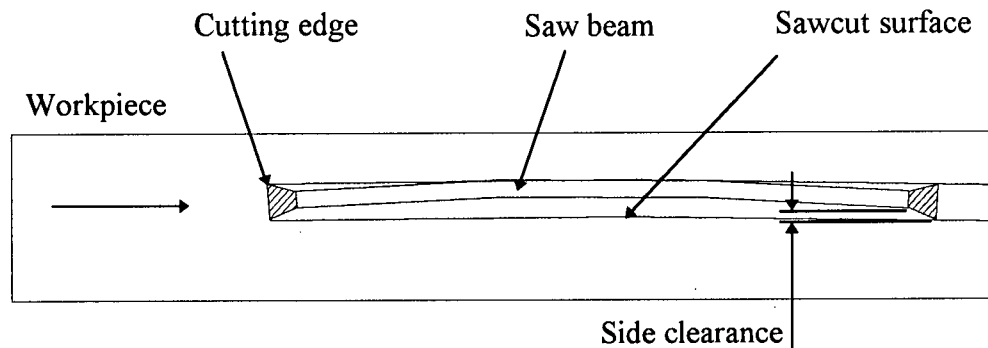
Figure 6.13: Beam Model Cutting and Interacting with a Workpiece

Whenever the workpiece starts to touch the beam surface, the local foundation stiffness is increased substantially to account for the new support to the beam. The displacement of the beam is then locally constrained to match the sawn surface at the contact points. This is done by applying the local sawn surface heights as foundation displacements, as described in Section 6.3.

The dimensions of the test saw corresponding to figure 6.1 are:

Outer diameter	0.750 m
Inner diameter	0.200 m
Plate thickness	0.002 m
Tooth side-clearance	0.0005 m
Young's modulus	200 G Pa
Density	7850 kg / m^3
Cutting height	0.100 m

Table 6.1: Dimensions of the Test Saw

From these dimensions, the following quantities were chosen for the beam model:

Length	0.750 m
Thickness	0.002 m
Width	0.200 m
EI	27 Pa.m^4
Mass per unit length	3.1 kg / m
Foundation stiffness (fixed-collar saw)	2 MN / m in middle $^1/_3$
Foundation stiffness (guided saw)	0.1 MN / m in front ¼
Feed speed	0.5 m / s

Table 6.2: Dimensions of the Saw Beam Model

Calculations were done for a fixed-collar saw and for a guided spline-arbor saw. These two saws had the same dimensions and were modeled by the same beam. The only difference was that the beam for the fixed-collar saw had a foundation stiffness that covered the middle one-third of the beam. This simulated the support provided by the saw collar. The guided spline-arbor saw had a foundation stiffness that covered the front one-quarter of the beam. This simulated the support provided by the guide. The sizes of the foundation stiffnesses used were chosen to give realistic deflected beam shapes and edge stiffnesses for the guided saw about double that of the fixed-collar saw. This represents typical saw properties [14]. The beam width was chosen to be twice the sawblade cutting height so that it would include some bending stiffness attributable to the areas of the circular saw above and below the cutting area.

Figure 6.14 shows calculated lateral deflections vs. time for a beam representing a fixed-collar saw. The lower curve shows the response due to a constant lateral (cutting) force of 1.0 N applied at the leading end. The resulting deflections are just less than the tooth side-clearance, and so minimal workpiece contact occurs on the downstream surface of

the beam. Therefore, the beam deflection remains constant, producing a straight but slightly offset sawcut surface. However, if the cutting force is increased to 1.5 N, the tooth deflection exceeds the side-clearance, and significant contact occurs. "Rudder" action starts to occur, and the workpiece irrecoverably pushes the beam to one side. The same behavior occurs even more rapidly for a cutting force of 2.0 N.

Figure 6.15 shows the corresponding displacements vs. time for a beam representing a guided spline-arbor saw. Here, the lower curve shows the response due to a constant lateral (cutting) force of 3 N applied at the leading end. As before, the resulting displacements are just less than the tooth side-clearance, and so minimal workpiece contact occurs on the downstream surface of the beam. However, the resemblance stops there. The curves in Figure 6.15 show that the sideways deflection of the leading edge of the beam continues to increase with increase in lateral force. However, the workpiece does not irrecoverably push the beam to one side. This is true even for the much larger cutting forces, 6N and 12 N.
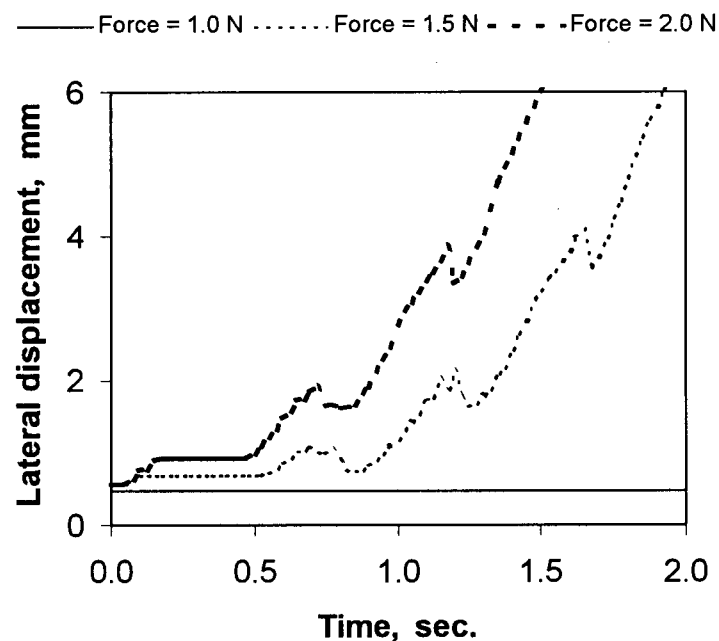
Figure 6.14: Calculated Sideways Displacements of a Beam Model of a Fixed-Collar Saw with Constant Lateral Forces at the Cutting Edge

Force = 3 N ········Force = 6 N ▪ ▪ ▪ ▪Force = 12 N
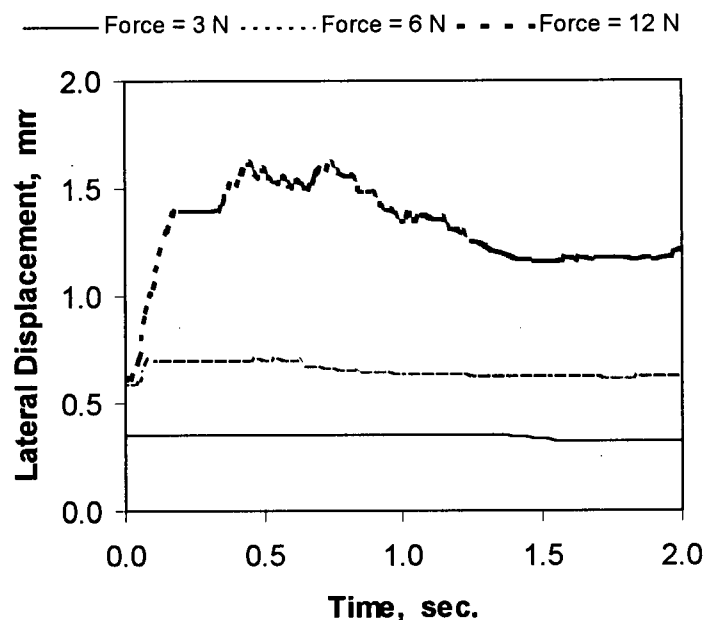
Figure 6.15:   Calculated Sideways Displacements of a Beam Model of a Guided Spline-arbor Saw with Constant Lateral Forces at the Cutting Edge

Figures 6.14 and 6.15 clearly demonstrate some fundamental differences between guided and fixed-collar saws. Firstly, the stiffness at the cutting edge is greater for the guided saw because the guide provides support the saw closer to its cutting edge. Secondly, the "rudder" action enables a guided saw to avoid being pushed irrevocably to one side, even if the cutting force is sufficient to cause sideways displacements much greater than the tooth side-clearance. In contrast, a fixed-collar is relatively flexible, and is not able to tolerate cutting forces greater than those that cause sideways deflections greater than the tooth side-clearance.

The simple beam model presented here gives a realistic representation of practical sawblade behavior. The sawblade behaviors illustrated in figures 6.14 and 6.15 clearly reflect the observations made during the experimental measurements done in this study. The experimental measurements confirmed that guided saws have a much greater cutting capacity (could run at larger gullet feed index) than fixed-collar saws. They cut more accurately, were stable over a wider operating range, and were not susceptible to rudder type instability.

7.0 Conclusions

This thesis presents an extensive experimental and theoretical study to investigate the key factors controlling guided circular saw cutting behavior and to provide insight into the design of improved guided circular saws. This study was motivated by previous observations that guided circular saw cutting behavior significantly differs from that of traditional unguided saws. It was suspected that this behavioral difference is due to the differing workpiece interactions of the two saw types. This study sequentially goes through a series of procedures including preliminary experimental studies, investigation of saw-workpiece interaction mechanisms, saw-workpiece interaction experimental studies and development of a theoretical model.

In some preliminary experimental studies, idling tests on a fixed-collar saw were conducted. Detailed information on fixed-collar and guided saw cutting behaviors was obtained by extensive wood-cutting experiments. Snaking saw, dished saw and stable saw areas were identified by using a contour plot of the standard deviations of the sawcuts, measured over a wide range of rotation speeds and thermal tensioning.

The behavior of an idling fixed-collar saw conforms to the theoretical expectations from the classical critical speed theory. The tendency of the cutting accuracy of a fixed-collar saw mirrors the vibration characteristics of an idling fixed-collar saw. In cutting tests with a fixed-collar saw, the standard deviation changes from a stable cutting area to critical speed and dishing areas are substantial and closely follow theoretical expectations.

Although the tendency of guided saw cutting accuracy is similar to that of a fixed-collar saw, a guided saw has a wider range of acceptable cutting accuracy. The standard deviations of a guided saw are relatively insensitive to tensioning. A guided saw can be stably operated at supercritical speeds. The behavior of a guided saw only weakly follows theoretical expectations from the traditional critical speed theory. A guided saw also has a much greater cutting capacity than a fixed-collar saw.

During investigation of the fundamental questions in the preliminary experimental studies, the following significant interactions between the saw and workpiece were observed:

- A fixed-collar saw became unstable during cutting, while the saw was stable when idling. Some interactions between the saw and workpiece must exist.

- During a light cut in the fixed-collar saw tests, the sawblade inclined to one side, overheated, became permanently bent and finally stopped. This occurred with a workpiece feed rate much lower than the rates that were easily handled by the same sawblade when mounted as guided saw. This suggests an important interaction between the saw body and workpiece.

From the previous experimental studies [3], the behavior of an idling guided saw fairly closely follows the expectations from traditional critical speed theory. The preliminary experimental studies show that a cutting guided saw only weakly follows the expectations from traditional critical speed theory. Therefore, during cutting the interaction between the saw and workpiece makes this difference.

Two aspects of saw-workpiece interaction are investigated. In extensive comparative cutting tests with various guide configurations, various combinations of three guides are successively used to identify the two aspects of saw-workpiece interaction. "Rudder" type behavior appears to be a primary factor that allows a guided saw to cut more accurately and to have a higher cutting capacity than a similar fixed-collar saw. The radial stresses that are induced during sawing may also influence the relative stability of counter-cutting and climb-cutting saws. The two saw-workpiece interaction mechanisms and the experimental results presented in the saw-workpiece interaction experiments support the ranking of the saw types listed in table 4.1. In general, guided saws cut more accurately than fixed-collar saws, and climb-cutting saws cut more accurately than counter-cutting saws. This ranking is recognized in modern industrial practice. Most new gangsaws installed in North American sawmills use climb-cutting guided saws.

For the saw-workpiece interaction experiments, further understanding of the interactions between the saw and workpiece may be achieved from the following points:

- In figure 5.7, the three guided counter-cutting saws show a substantial reduction in sawing standard deviations compared with a fixed-collar saw. On the left side of the critical speed, the "rudder" action shown in figure 4.3 and 4.4 limits the sideways motion of the guided saws so that the cutting accuracy is superior to that of a fixed-collar saw.

- For a dished guided counter-cutting saw, the "rudder" mechanism shown in figures 4.3 and 4.4 limits the sideways motion of the downstream part of the saw so that the cutting accuracy is substantially improved.

- For a dished fixed-collar counter-cutting saw, the cutting edge of the saw moves to one side. The "rudder" mechanism shown in figures 4.1 and 4.2 further helps this movement so that the cutting accuracy deteriorates quickly, as shown in figure 5.7.

- In figure 5.7, the gullet feed index of the fixed-collar saw is only one third of that possible with the guided saw for the same minimum standard deviation. This supports the "rudder" action as an important mechanism to describe the interaction between the saw body and workpiece.

- For the three counter-cutting guided saws in figure 5.7, the massive guiding using guides on both sides of a saw is detrimental to improving cutting accuracy on the left of the curves. This is because the additional guide on the outfeed side limits the "rudder" action of the saw.

- Contrary to expectations based on saw stiffness, a guided saw with quite small guides can cut wood accurately, as shown in figure 5.7. In a curve sawing system, a guided saw with smaller guides is more flexible and can increase the "rudder" action so as to allow the flexible saw body to follow the cutting edge more easily and accordingly cut more accurately.

- From figure 5.9, the cutting standard deviations of climb-cutting saws are much lower than those of the counter-cutting saws and almost independent of

sawing conditions. Saw critical speed instability and saw dishing do not have obvious influence on their sawcut standard deviations. These support that the interaction between saw tooth and workpiece shown in figure 4.5 is an important factor that controls guided saw cutting behavior.

- The climb-cutting saw vibration curves in figure 5.11 show a notable interaction example. The climb-cutting saw oscillates greatly from side to side during idling, but this oscillation decays or entirely disappears during cutting. This is a dramatic demonstration of the effect of saw interaction with the workpiece.

- The climb-cutting saw shown in figure 5.11 becomes stable during cutting, but the counter-cutting saw shown in figure 5.10 becomes less stable during cutting. These effects may be related to tensile/compressive radial stresses caused in the interaction between the saw tooth and workpiece.

The theoretical model presented in this thesis complements the experimental results and further supports the interaction mechanisms. The "rudder" action is demonstrated in the cases of a fixed-collar saw and a guided saw. The theoretical model provides an important tool for further understanding of the interaction between the saw and workpiece. In this model, necessary saw cutting factors have been gradually added. A computer program is used to implement this model. This can model the "rudder" action.

In summary, the main contributions of this study are:

1. In the preliminary experimental studies, it is further verified that a fixed-collar saw closely follows theoretical expectations, but easily bends out of line on heavy cuts.

2. In the preliminary experimental studies, it is shown that a guided saw only weakly follows theoretical expectations, has a much greater cutting capacity and can be stably operated at supercritical speeds.

3. From the preliminary experimental studies, significant interaction between the saw and wood is observed. This interaction is identified as an important factor that controls how guided saws work and therefore is a significant saw design factor.

4. Further investigation and extensive experiments on two aspects of saw-workpiece interaction support that the interaction between the saw and workpiece definitely is a key factor controlling guided saw cutting behavior and is a significant saw design factor. "Rudder" type behavior and the radial stresses of a cutting saw are identified as two main factors in considering how guided saws work and designing guided saws.

5. For the ranking of the saw types, it is identified that guided saws cut more accurately than fixed-collar saws, and climb-cutting saws cut more accurately than counter-cutting saws.

6. The differing "rudder" actions of guided and fixed-collar saws can be successfully demonstrated using a simplified theoretical model based on a beam on an elastic foundation.

Suggestions for Future Work

1. Further studies are needed to investigate the significance of radial stresses on sawing stability of counter-cutting and climb-cutting saws. It is likely that some measurements of the cutting forces in the counter-cutting and climb-cutting are needed to conduct this work.

2. Further experimental studies including some practical industrial tests are needed to answer the question of whether or not it may be necessary to reduce industrial guide size to encourage "rudder" action.

3. The theoretical model needs to be developed further so that it can model sawblade interaction with the workpiece more fully.

References

1. Yang, L. "Supercritical Speed Response of Circular Saws." MASc Thesis, The University of British Columbia, Vancouver, B.C. 1990.

2. Schajer, G. S. and Kishimoto, K. J. "High-Speed Circular Sawing Using Temporary Tensioning." Holz als Roh- und Werkstoff, Vol. 54, pp.361-367. 1996.

3. Schajer, G. S. and Kishimoto, K. J. "Non-classical Critical Speed Behavior of Guided Circular Saws." Proc. 13th International Wood Machining Seminar, Vancouver, Canada. June 1997.

4. Lister, Peter F. and Hutton, S. G. and Kishimoto, K. J. "Experimental Sawing Performance Results for Industrial Supercritical Speed Circular Saws." Proc. 13th International Wood Machining Seminar, Vancouver, Canada. June 1997.

5. Dugdale, D. S. "Stiffness of a Spinning Disk Clamped at its Center." Journal of the Mechanics and Physics of Solids, Vol. 14, pp.349-356. 1966.

6. Schajer, G. S. "Circular Saw Tensioning: What It Is, Why It Matters." Sawing Technology, May 1989.

7. Campbell, W. "The Protection of Steam Turbine Disc Wheels From Axial Vibration." Transactions of the ASME, Vol.46, 1924, pp. 31-160. 1924.

8. Mote, C. D. "Circular Saw Stability." Forest Prod. J., Vol.16 No.6, pp. 244-250. 1964.

9. Mote, C. D. "Stability of Circular Plates Subjected to Moving Loads." J. Franklin Inst. Vol.290 No.4, pp. 329-344. 1970.

10. Mote, C. D. and Szymani, R. "Principal Developments in Thin Circular Saw Vibration and Control Research: Part 1: Vibration of Circular Saws." Holz als Roh- und Werkstoff, 35, 1977, pp. 189-196. 1977.

11. Szymani, R. and Mote, C. D. "Principal Developments in Thin Circular Saw Vibration and Control Research: Part 2: Reduction and Control of Saw Vibration." Holz als Roh- und Werkstoff, 35, 1977, pp. 219-225. 1977.

12. Mote, C. D., Schajer, G. S., and Holøyen, S. "Circular Saw Vibration Control by Induction of Thermal Membrane Stresses." Journal of Engineering for Industry, Vol. 103, No.1, pp. 81-89. 1981.

13. Schajer, G. S. "Guided Saw Hunting." Forest Products Journal, Vol. 38, No. 4, pp. 47-50. 1988.

14. Schajer, G. S. "Why Are Guided Circular Saws More Stable Than Unguided Saws?" Holz als Roh- und Werkstoff, 44, 1986, pp. 465-469. 1986.

15. Schajer, G. S. "Guided Circular Saw Critical Speed Theory." Proceedings of SawTech '89, Oakland, California, October 2-3. 1989.

16. Schajer, G. S. "Vibration Modes of Guided Circular Saws." Proc. 10th International Wood Machining Seminar, Berkeley, CA, October, 1991.

17. Hutton, S. G., Chonan, S., and Lehmann, B. F. "Dynamic Response of a Guided Circular Saw." Journal of Sound and Vibration, Vol.112, No.3, pp. 527. 1987.

18. Lehmann, B. F. and Hutton, S. G. "Self-Excitation in Guided Circular Saws." Trans ASME, J. of Vibration, Acoustics, Stress, and Reliability in Design, July 1988, Vol. 110, pp. 338. 1988.

19. Hutton, S. G. "The Dynamics of Circular Saw Blades." Holz als Roh- und Werkstoff, Vol. 49, pp. 105-110. 1991.

20. Yang, L. and Hutton, S. G. "Interactions Between an Idealized Rotating String and Stationary Constrains." Journal of Sound and Vibration, Vol. 185, No. 1, pp. 139-154. 1995.

21. Mote, C. D. and Nieh, L. T. "On the Foundation of Circular Saw Stability Theory." Wood and Fiber, Vol. 5, No. 2, pp.160-169. 1973.

22. Schajer, G. S. "The Vibration of a Rotating Circular String Subject to a Fixed Elastic Constraint." Journal of Sound and Vibration, Vol. 92, No. 1, pp.11-19. 1984.

23. Carlin, J. F., Appl, F. C., Bridwell, H. C. and Dubois, R. P. "Effects of Tensioning on Buckling and Vibration of Circular Sawblades." Journal of Engineering for Industry, Vol. 2, No. 1, pp.37-48. 1975.

24. Englesson, T. Hvamb, G. and Thunell, B. "Some Results from Counter and Climb Ripsawing Investigations." Meddelelse Nr. 7, Norsk Treteknisk Institutt, Oslo. Norway. 1954.

25. Lehmann, B. F. Personal Communication. Thin-Kerf Technologies, Vancouver, Canada. 1998.

26. Lister, P. F. Personal Communication. Forintek Canada Corporation. Vancouver, Canada. 1998.

27. Martin, H. C. "Introduction to Matrix Methods of Structural Analysis." McGraw-Hill, Toronto. 1966.

28. Singer, F. L. "Strength of Materials." Second Edition. Harper & Row, New York. 1962.

29. Timoshenko, S. "Strength of Materials. Part I. Elementary Theory and Problems." Third Edition. Krieger, Malabar, Florida. 1958.

30. Timoshenko, S. "Strength of Materials. Part II. Advanced Theory and Problems." Third Edition. Krieger, Malabar, Florida. 1958.

31. Young, Warren C. "Roark's Formulas for Stress and Strain." Sixth Edition. McGraw-Hill, New York. 1989.

32. Dimarogonas, A. "Vibration for Engineers." Second Edition. Prentice-Hall, New Jersey. 1996.

33. Sack, R. A. "Transverse Oscillations in Travelling Strings." British Journal of Applied Physics. Vol. 5. pp. 224-226. 1954.

34. Dongarra, J. J. et al. "Linpack: Users' Guide." SIAM, Philadelphia. 1979.

35. Maness, Thomas C. and Lin, Y. "The Influence of Kerf and Target Size Reductions on Sawmill Revenue and Volume Recovery." Proceedings of SawTech '95, Seattle, Washington, U.S.A., October 26-27, 1995.

Appendix

1. Feed Speeds and Feed per Tooth of a Fixed-Collar Saw in Preliminary Experiment

In the cutting tests, the feed per tooth of each rotation speed was adjusted to be 0.053". The gullet feed index was maintained at 0.09. The following table lists feed speeds and corresponding saw rotation speeds:

Saw Rotation Speed (rpm)	800	1000	1200	1400	1600	1800
Feed Speed (fpm)	113.9	142.4	170.9	199.4	227.8	256.3

2. Feed Speeds and Feed per Tooth of a Guided Saw in Preliminary Experiment

In the cutting tests, the feed per tooth of each rotation speed was adjusted to be 0.039". The gullet feed index was maintained at 0.25. The following table lists feed speeds and corresponding saw rotation speeds:

Saw Rotation Speed (rpm)	800	1000	1200	1400	1600	1800
Feed Speed (fpm)	84.4	105.5	126.6	147.7	168.8	189.9

3. Feed Speeds and Feed per Tooth of Guided Saws in Saw-Workpiece Interaction Experiments

In the cutting tests, the feed per tooth of each rotation speed was adjusted to be 0.047". The gullet feed index was maintained at 0.30. The following table lists feed speeds and corresponding saw rotation speeds:

Saw Rotation Speed (rpm)	600	800	1000	1200	1400	1600	1800	2000
Feed Speed (fpm)	75.9	101.3	126.6	151.9	177.2	202.5	227.8	253.2